Investigation of Inlet and Entry Region Characteristics on the Discrete Passage Diffuser Pressure Rise Performance

by

Yongcheng Liang

S.B. Tsinghua University, Beijing, June 1989

Submitted to the Department of Aeronautics and Astronautics
in partial fulfillment of the requirements for the degree of

Master of Science in Aeronautics and Astronautics

at the

MASSACHUSETTS INSTITUTE OF TECHNOLOGY

September 1994

Author .....
Department of Aeronautics and Astronautics
July 11, 1994

Certified by .....
Professor Edward M. Greitzer
H. N. Slater Professor of Aeronautics and Astronautics
Thesis Supervisor

Accepted by .....
Professor Harold Y. Wachman
Chairman, Department Graduate Committee

Investigation of Inlet and Entry Region Characteristics on the Discrete Passage Diffuser Pressure Rise Performance

by

Yongcheng Liang

Submitted to the Department of Aeronautics and Astronautics on July 11, 1994 in partial fulfillment of the requirement for the Degree of Master of Science

Abstract

A study of data from two discrete passage diffusers has been carried out, with emphasis on inlet and entry region characteristics. A wide range of inlet conditions has been examined. The total pressure loss occurring in the diffuser entry region has been quantified, as has the throat blockage. If the total pressure loss in the entry region is taken into account, it is found that the performance of the channel part of the diffuser(i.e. from diffuser throat to diffuser exit) has a dependence on throat blockage that is similar to two dimensional diffusers. Throat blockage was found to be dependent on inlet swirl angle with little dependence on inlet blockage. The latter thus exerts little influence on the overall pressure rise of the discrete passage diffuser.

Acknowledgments

Over the past two years, a lot of support and encouragement was given to me by so many that it is hard for me to know where to begin.

First, I would express my grateful thanks to my thesis advisor, Professor Greitzer, whose guidance in both fluid mechanics and in discerning important results from raw data was always essential.

Also I would like to thank Dr. Choon Tan for his thought provoking comments and advice.

Dr. Gerald Guenette's expert advice on everything is also greatly acknowledged.

Dr. Sabri Deniz's provoking comments and expert advice is also appreciated.

I also like to express my grateful thanks to Bill Ames, James Letendre and Viktor Dubrowski, without whose help my work would have been impossibly difficult.

I also want to thank John Mark Johnston, whose generous support and effort made my life much easier.

I also feel indebted to the G.T.L. student group, they are always ready to offer help or advice when you need it even if they are busy with their own projects.

The Gas Turbine Laboratory provided the framework to pursue research in the guise of: Holly Rathbun, Jean Anderson, Diana I. Park, Robin Courchesne on the administrative side. I thank you all.

This research was supported by the Army Research Office through Grant #03-90 G-0138, under direction of Dr. Thomas Dalagalski, technical monitor and by Kobe Steel Ltd.,Dr. Fumikata

Kano, technical monitor. Their support is gratefully appreciated.

Last, but not least, I would like to thank my wife, Hong Shu, for her moral support.

TABLE OF CONTENTS

LIST OF TABLES

LIST OF FIGURES

Nomenclature

Symbols

A	area
α	swirl angle at the inlet
B	blockage
Cp	static pressure rise coefficient
Cp_Ψ	static pressure rise coefficient based on availability averaged diffuser inlet dynamic pressure
k	ratio of specific heats, Cp/Cv
m	mass flow rate
M	Mach number
P	static pressure
P_t	total pressure
$P_{t\Psi}$	availability-averaged total pressure
ρ	static density
r	radius
R	gas constant for air in equation of state $Pv=RT$
T	static temperature
T_0	total temperature
V	velocity
Z	vane number of a diffuser

Subscripts		
0	" total" for temperature	
1	diffuser inlet	
2	diffuser exit	
act	actual	
corr	corrected	
r	radial direction	
ref	reference	
t	" total" for pressure	
th	diffuser throat	
tth	"throat total"	
θ	tangential direction	

Chapter 1

Introduction and Background

1.1 Introduction

The flow leaving the impeller of a centrifugal compressor is generally inclined at a large angle to the radial direction. To decelerate the flow and achieve a desired pressure rise, a properly designed diffuser must be placed downstream of the impeller.

The diffuser configurations applied to centrifugal compressors can be grouped roughly into two types. Vaneless diffusers, which are used when wider range or lower cost are of prime concern, and vaned diffusers, which are used when maximum pressure rise and efficiency are needed or geometric constraints make it impossible to use a vaneless diffuser. A variant of the vaned diffusers, used for high performance turbomachinery, is the discrete passage diffuser. They are viewed as exhibiting a higher pressure-recovery characteristic than the vaned diffusers, although little data on this point exists in the open literature. There is also a lack of knowledge about flow mechanisms inside such discrete passage diffusers to aid in generating a systematic approach to diffuser design.

Information concerning discrete passage diffuser performance is scarce. and a comment made by Dean some time ago still appears to be true, Dean made the following statement about vaned diffusers, " ..... So far in our experience, we can find no preferred dogma for the vaned

diffuser design, except that the United Aircraft of Canada pipe diffusers seem to give consistently better peak recovery, but often shorter range. This may not be because theirs is an inherently superior design (although we do feel it contains many desirable features such as boundary layer fences in the semi-vaneless region), but may be because the pipe diffuser family is more tractable during the design process ..... " [4].

To clarify some of the issues concerning the flow in centrifugal diffusers, we have examined experimental data acquired over the past several years at the Gas Turbine Lab. The focus is on flow mechanisms inside the entry region, especially those which affect the pressure recovery performance. The main effort is aimed at computing the total pressure loss inside the entry region and investigating how throat blockage affects the pressure recovery.

1.2 Background

As pointed out by Wilson [15], one of the main problems in predicting centrifugal compressor diffuser performance is that the flow at the exit of the impeller is typically not only non-uniform, but often has characteristics unique to that particular impeller design. To fully understand the flow mechanism and predict the performance of a diffuser at the design stage, several issues must be addressed. One is to provide instrumentation between the impeller and diffuser which can give the required measurements in this distorted flow field. A second and more difficult problem is to isolate and identify the prime

parameter(s) associated with the inlet flow which determine(s) the performance of the diffuser.

The parameters of the flow at the diffuser inlet include Mach number, inlet swirl angle, inlet blockage and parameter expressing the non-uniformity of the momentum, kinetic energy, and flow angle. To investigate the impact of inlet flow conditions, Filipenco designed and constructed a test facility [7], using a high solidity swirl generator, which provided a controlled inlet flow for the diffuser downstream of the swirl generator. Filipenco also examined different ways to characterize diffuser performance. He stated that various investigators had correlated their data in terms of different parameters, some of which had ambiguous physical significance. Further some results were not applicable to other configurations due to inappropriate averaging methods to describe inlet flow profiles. Filipenco used an availability averaged total pressure, defined as:

$$\overline{P_{t\psi 1}} = \exp \frac{\int_0^b \ln(P_{t1})\, \rho_1 V_{r1} 2\pi r_1 dx}{\int_0^b \rho_1 V_{r1} 2\pi r_1 dx} \qquad (1.1)$$

This is the maximum total pressure which can be attained in an ideal process in an isolated system that ends in a uniform zero velocity state.

The total pressure defined in Equation 1.1 was used to define the pressure recovery coefficient as:

$$Cp_\psi = \frac{P_2 - P_1}{\overline{P_{t\psi 1}} - P_1} \qquad (1.2)$$

The pressure recovery coefficient indicates to what extent the dynamic pressure of the flow at the inlet to the diffuser is converted into static

pressure by the diffuser. For an ideal flow (isentropic, one dimensional), the maximum value this coefficient can reach is unity. The entropy and total pressure of the flow through the diffuser would then be uniform and the static pressure at the diffuser exit would be equal to the availability average total pressure at the diffuser inlet. For a real diffuser, Cp will be less than unity.

Filipenco also introduced momentum averaged inlet flow velocity components, defined as:

$$\overline{V_{\theta 1}} = \frac{\int_0^b \rho_1 V_{r1} V_\theta 2\pi r_1 dx}{\int_0^b \rho_1 V_{r1} 2\pi r_1 dx} \qquad (1.3)$$

and

$$\overline{V_{r1}} = \frac{\int_0^b \rho_1 V_{r1} V_r 2\pi r_1 dx}{\int_0^b \rho_1 V_{r1} 2\pi r_1 dx} \qquad (1.4)$$

Using Equation 1.3 and Equation 1.4, the momentum averaged inlet flow angle was defined as:

$$\overline{\alpha_1} = \arctan\left(\frac{\overline{V_{\theta 1}}}{\overline{V_{r1}}}\right) \qquad (1.5)$$

Filipenco's results showed that different inlet velocity and flow angle distributions and inlet blockage conditions could be collapsed by using the inlet momentum averaged swirl angle. The pressure rise coefficient of his discrete passage diffuser, shown in Figure 1-1, was then given as a function of the inlet momentum averaged swirl angle.

While these results are extremely useful, they leave unanswered

the question of why the flow behaves the way it does. In a two dimensional diffuser, the pressure recovery coefficient of the diffuser depends on the inlet blockage. As inlet blockage goes up, pressure recovery coefficient goes down. If we assume the channel of the discrete passage diffuser behaves as a two dimensional diffuser, two related problems are of interest. One is to relate the swirl angle to the ratio of effective throat area to inlet flow streamtube area. The second is to show that when the throat blockage (although not necessarily the inlet blockage) goes up, the static pressure recovery coefficient does indeed decrease.

1.3 Fluid Dynamic Questions to be Addressed

The following fluid dynamic questions were addressed:

- Why does diffuser pressure rise coefficient, defined in Equation 1.2, depend on the inlet swirl angle alone?
- How is throat blockage related to inlet blockage? What is the role of mixing in relating these?
- What is the total pressure loss in the entry region of a discrete passage diffuser?
- How can we best interpret the pressure rise characteristic of the discrete passage diffuser and relate it to other diffuser data?

1.4 Objectives and Contributions of the Present Research

We can restate the above questions as leading to the following objectives:

1. What is the underlying reason that the pressure rise coefficient of a discrete passage diffuser is a function of momentum averaged inlet swirl angle only?
2. How is throat blockage affected by inlet flow parameters?
3. What is the role of throat blockage in determining the performance of the channel after the throat of a diffuser? Does the channel of the diffuser behave the same way as a conventional two dimensional straight channel diffuser?
4. What is the magnitude of the total pressure loss in the entry region of a discrete passage diffuser for the geometries of interest? How is the loss affected by the inlet conditions?
5. What are the prime factors in determining the magnitude of the entry region total pressure loss?
6. Given the inlet flow and the geometry of a discrete passage diffuser, is there a simple and accruate way to predict the pressure rise of the diffuser?

The main contributions of this research may be listed as follows:

1. The throat blockage of a discrete passage diffuser was shown to depend mainly on momentum averaged inlet swirl angle, rather

than inlet blockage.

2. The total pressure loss in the entry region of a discrete passage diffuser has been computed and used in defining the pressure rise coefficient from diffuser throat to diffuser exit. This enable one to show that the channel of a discrete passage diffuser behaves similarly to two dimensional diffusers.
3. The pressure rise coefficient for the leading edge to the throat of a discrete passage diffuser and for the throat to the exit, found to be mainly determined by the momentum averaged inlet swirl angle. This explains why the overall pressure rise coefficient is only a function of the inlet momentum averaged swirl angle, as found by Filipenco.
4. A simple method has been developed to approximately predict the pressure rise of a discrete passage diffuser.

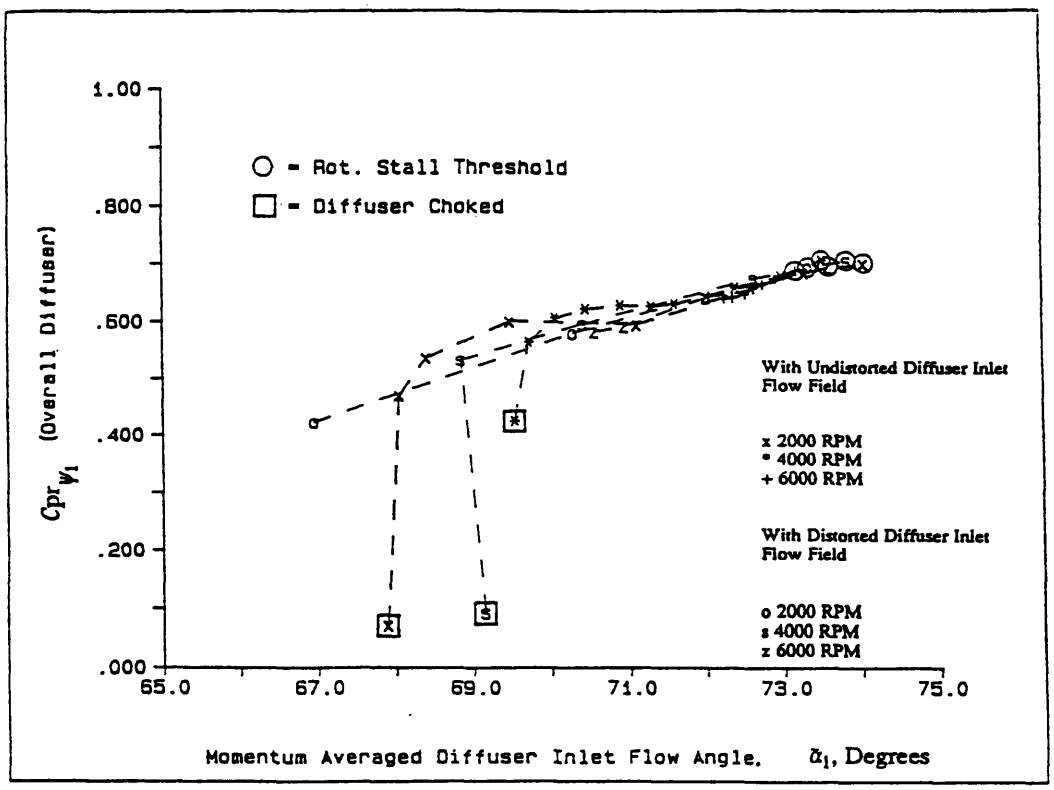

Figure 1.1 : Diffuser Overall, Availability Averaged Pressure Recovery, Cp_{ψ}, as a Function of Momentum Averaged Inlet Swirl Angle [7].

Chapter 2

Facility and Experimental Apparatus

2.1 Overall Facility Description

The test facility has been described fully by Filipenco [7] and only brief description is given here. The facility illustrated in Figure 2.1 consists of a very high solidity rotating radial outflow nozzle cascade(VHS-RRONC) with forward-leaning blades, which is driven directly by a variable AC induction motor. There are continuous circumferential slots immediately upstream and downstream of the rotor blading in the stationary walls. These control the inlet boundary layer blockage and profile distortion of the flow delivered by the swirl generator to the diffuser.

Downstream of the diffuser, the diffuser flow is dumped into a plenum with a throttle immediately downstream of the plenum. The mass flow normally can be monitored by the throttle, but a slave compressor can be activated to lower the diffuser back pressure if needed. Figure 2.2 shows the overall layout of the facility. The swirl generator mechanical-concept schematic is shown in Figure 2.3. Figure 2.4 provides a detailed view of the mass injection and suction paths. The amount of flow injection/suction of the four annular chamber can be controlled independently. Table 2.1 shows facility dimension parameters.

2.2 Discrete Passage Diffuser

The diffuser can be separated into four parts: the pseudo-vaneless space, leading to the throat, the throat and the diffusing cone. Diffusers are defined along a centerline, inclined at an angle from radial. The diffusing cone can have a range of length to inlet diameter ratios as the inclination angle of the passage and the throat area can both be varied. The diffuser geometry is shown in Figure 2.8a [4]. It is not expected that the shape of the diffusing cone helps the diffuser have higher pressure recovery over a vaned diffuser because Runstadler has shown that the peak recovery of conical and straight-channel diffusers is almost identical, Figure 2.9 [1]. The figure shows that maximum pressure recovery versus throat blockage for conical diffuser and straight-channel diffuser.

The diffuser examined in M.I.T. Gas Turbine Lab is shown in Figure 2.10 [7]. It was designed by GE Aircraft Engine Company. The specific diffuser parameters of the two diffusers examined by Filipenco and Johnston are given in Table 2.3

2.3 Instrumentation

At the impeller inlet, there is a thermocouple (type T) to measure inlet temperature. At the exit of the swirl generator, a single hole probe, shown in Figure 2.5, is installed. This can be rotated to provide the swirl angle and total pressure profile. The mass flow rate is measured by a Universal Venturi Tube, part number 0182 - 10 - 2291, located in the test-rig exit ten-inch. The rated uncalibrated accuracy of the flowmeter is

±1.0 % of true value. Total temperature at diffuser exit is measured by means of a shielded type E thermocouple probe. The swirl generator rotor speed was measured by means of a Shimpo model number DT-5BC digital readout tachometer, with readout resolution of 0.1 RPM.

One passage, for each diffuser (30 and 38 passage), had a line of seventeen static pressure taps placed along the centerline, with two in the throat region. There were also eight taps in the pseudo-vaneless space, and three additional taps at the diffuser exit. Figure 2.6 and Figure 2.7 [7] give pictures of the tap locations mentioned for the two diffusers tested. Specific geometric parameters of each tap were given in Table 2.2. There were also twelve taps placed around the inlet of the diffuser, six on each wall. A high response transducer was installed in the plenum. With the 30 passage diffuser three high response static pressure transducers were installed in the vaneless ring. Five more were added for the 38 passage diffuser testing.

2.4 Definition of Stations Used

"Plane 1" is the swirl generator radius, which is the traverse probe radius. "Plane 0" is the exit radius of the impeller. "Plane th" is the throat of the diffuser. "Plane 1A" is the radius at which the diffuser inlet circumferential static taps are placed. "Plane 2" is the diffuser exit radius immediately upstream of the dump to the plenum.

The axial direction is taken from the impeller hub, x=0, to the shroud, x=b. The flow swirl angle is defined as the angle from the radial direction, rather than from the tangential direction.

Table 2.1: Main Facility Dimension Parameters

	Quantity	Dimension	
1	Impeller Radius	7.26	inches
2	Impeller Width	0.354	inches
3	Blade Number of the Impeller	71	
4	Impeller Design Exit Angle	64	degrees
5	Impeller Design Exit Mach Number	0.8	
6	Swirl Generator Exit Radius	8.200	inches
7	Traverse Probe Diameter	0.039	inches
8	Traverse Probe Installed Radius	8.001	inches
9	Diffuser Inlet Static Tap Radius	8.201	inches
10	Universal Venturi Throat Diameter	5.81	inches
11	Exit Pipe Diameter	10.0	inches

Table 2.2: Diffuser Static Pressure Tap Locations

Tap No.	ξ	ζ	Tap No.	ξ	ζ
1	0.803	0.057	16	3.393	0.0
2	1.023	0.083	17	3.850	0.0
3	1.314	0.102	18	4.300	0.0
4	1.544	0.134	19	4.750	0.0
5	1.250	0.0	20	5.210	0.0
6	1.540	0.0	21	5.660	0.0
7	1.837	0.0	22	6.200	0.0
8	1.637	-0.071	23	6.693	0.0
9	2.131	0.0	24	7.186	0.0
10	1.927	-0.084	25	7.186	0.0
11	2.424	0.0	26	7.186	-0.275
12	2.218	-0.092	27	7.186	0.275
13	2.846	0.0	28	7.490	0.0
14	2.519	-0.113	29	7.728	-0.230
15	3.268	0.0	30	7.952	-0.460

Table 2.3: Dimensions of the Two Examined Discrete Passage Diffusers

Item	30 Passage Diffuser	38 passage Diffuser
Inlet Radius	7.982 inches	7.982 inches
Inlet Width	0.354 inches	0.354 inches
Exit Radius	11.046 inches	11.046 inches
Diffuser Throat Diameter	0.5057 inches	0.4493 inches
Total Throat Area	6.025 SQ. inches	6.025 SQ. inches
Total Exit Area	25.85 SQ. inches	26.33 SQ. inches
Geometric Inlet Angle	69 degrees	70.1 degrees
Area ratio	4.29	4.37
Diffuser L/D	8.75	9.44

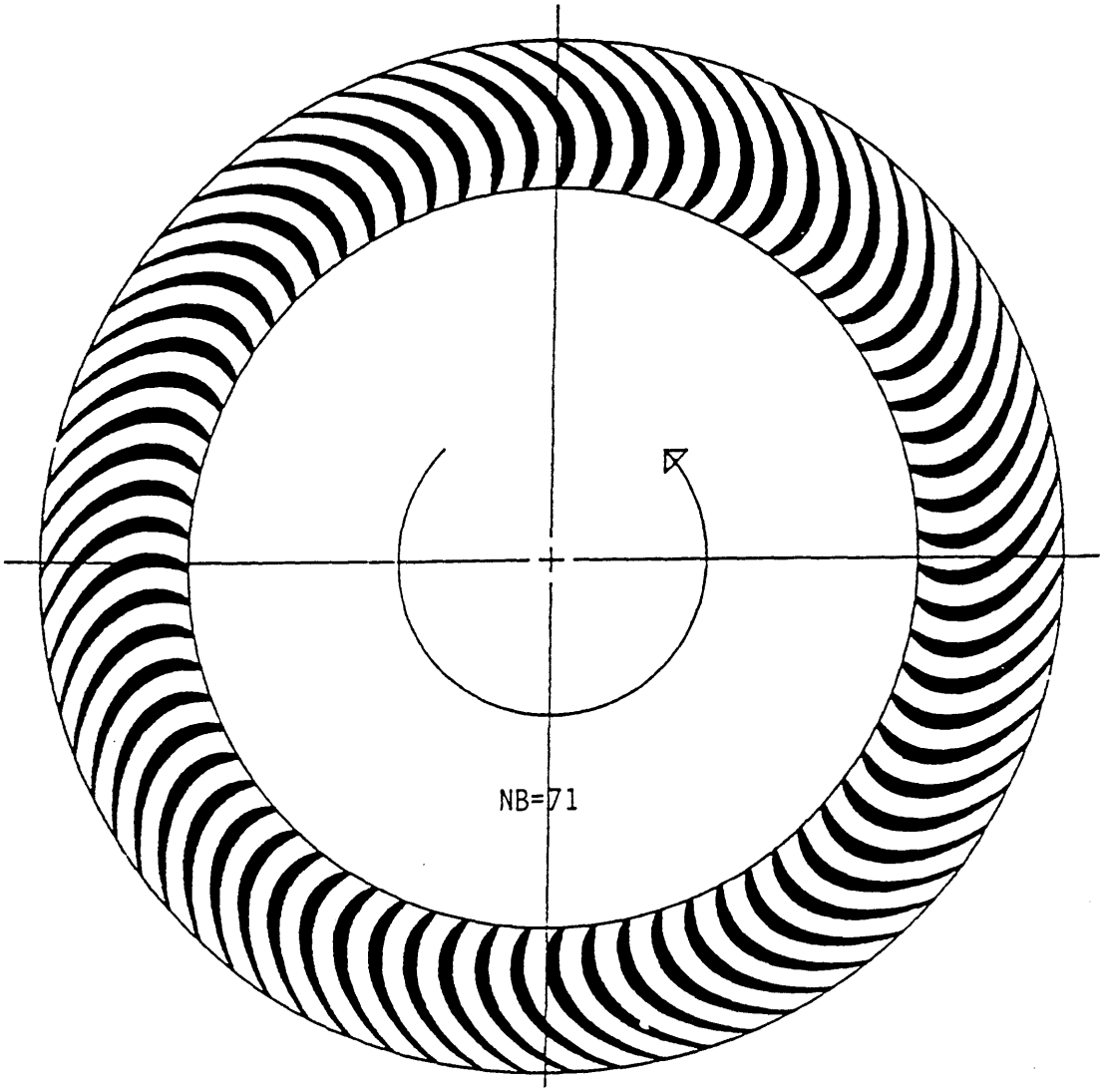

Figure 2.1: Impeller Blade Shape for (VHS-RRONC) [7].

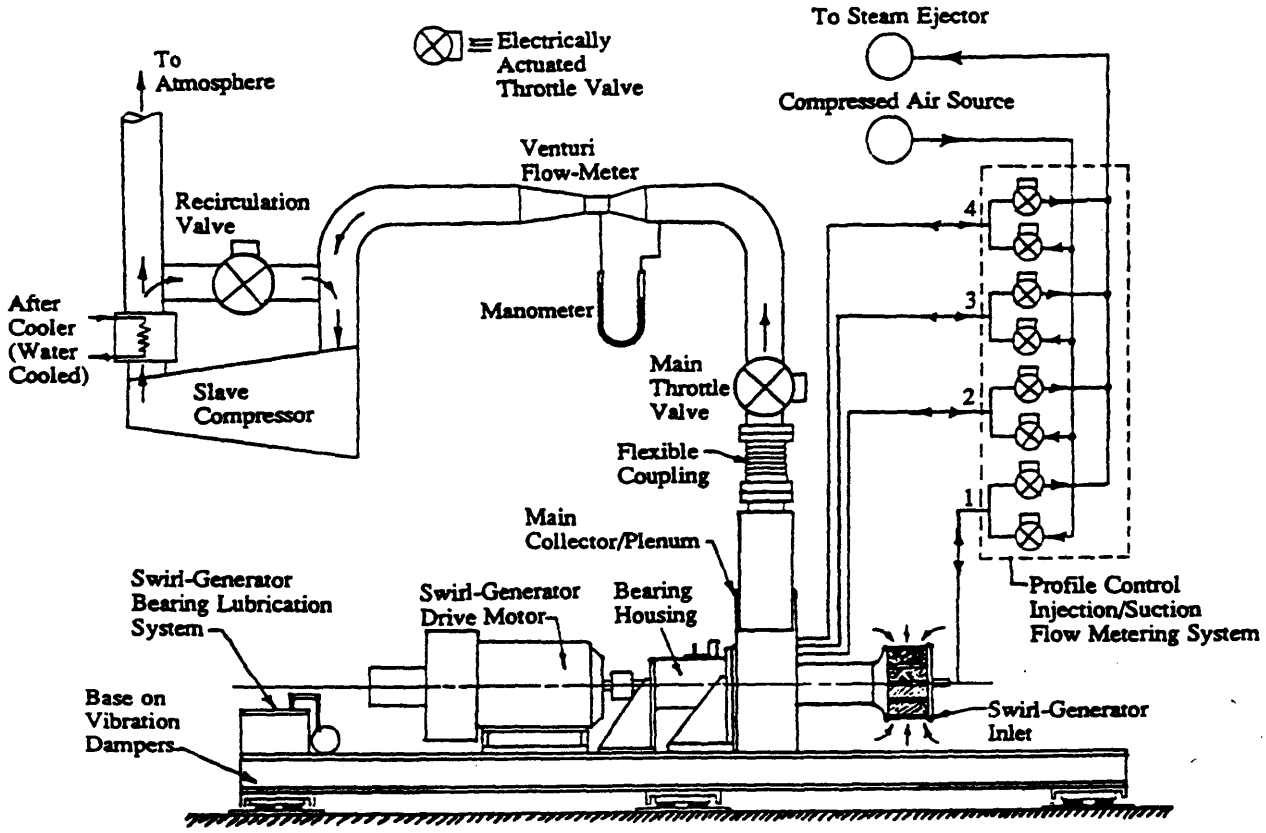

Figure 2.2: Piping Schematic [7]

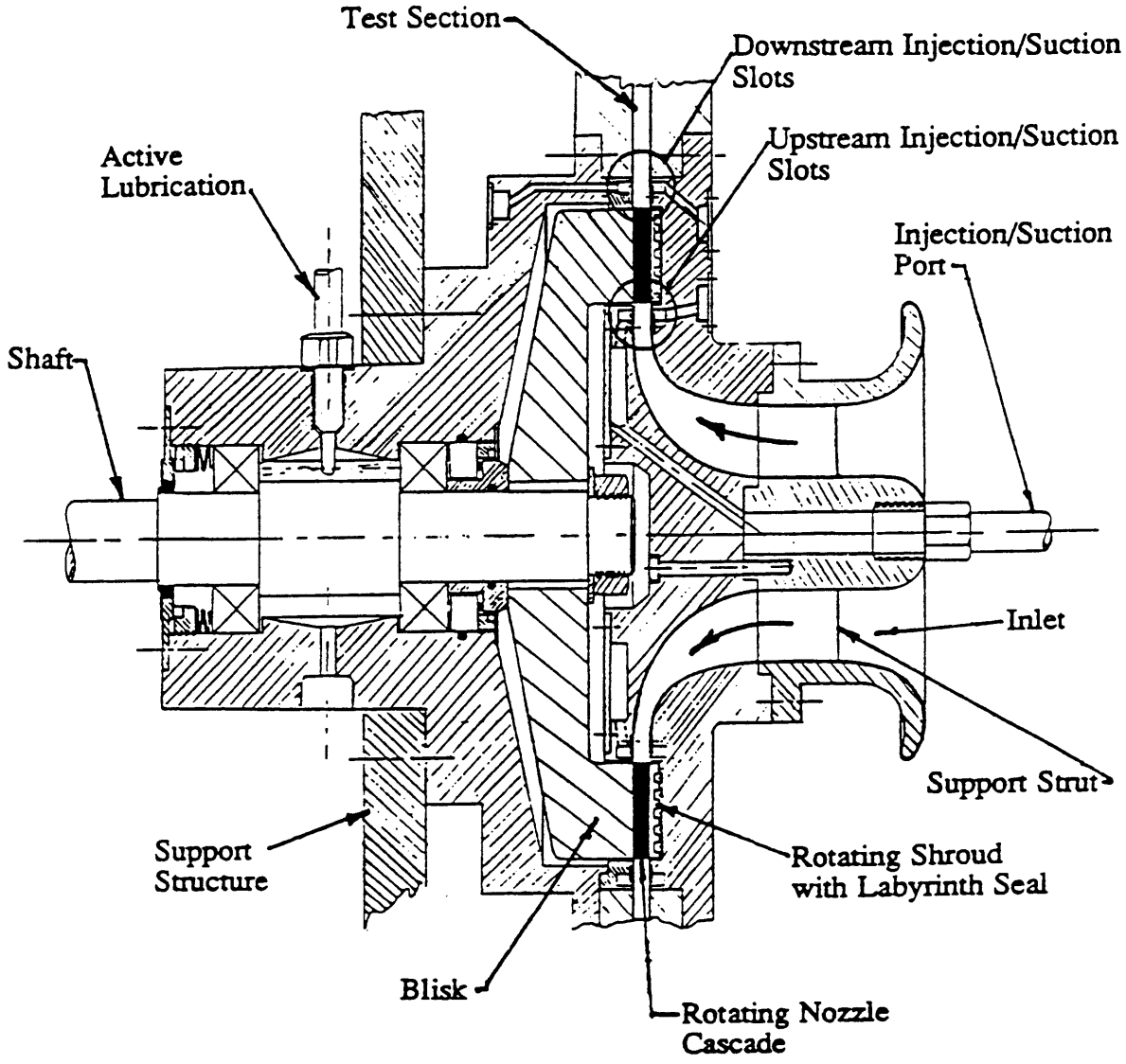

Figure 2.3: Swirl Generator Schematic [7]

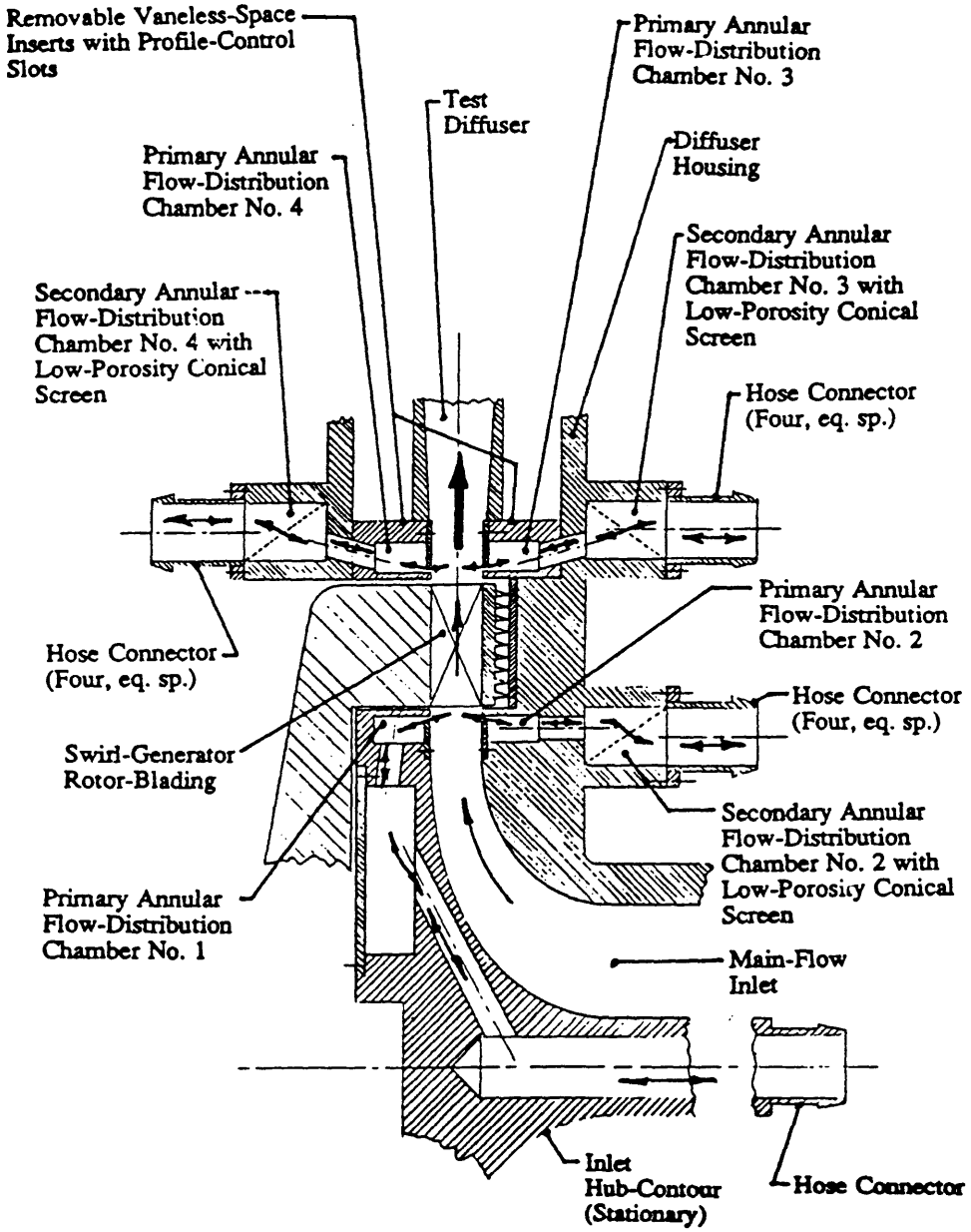

Figure 2.4: Mass Injection and Suction Flow Paths [7].

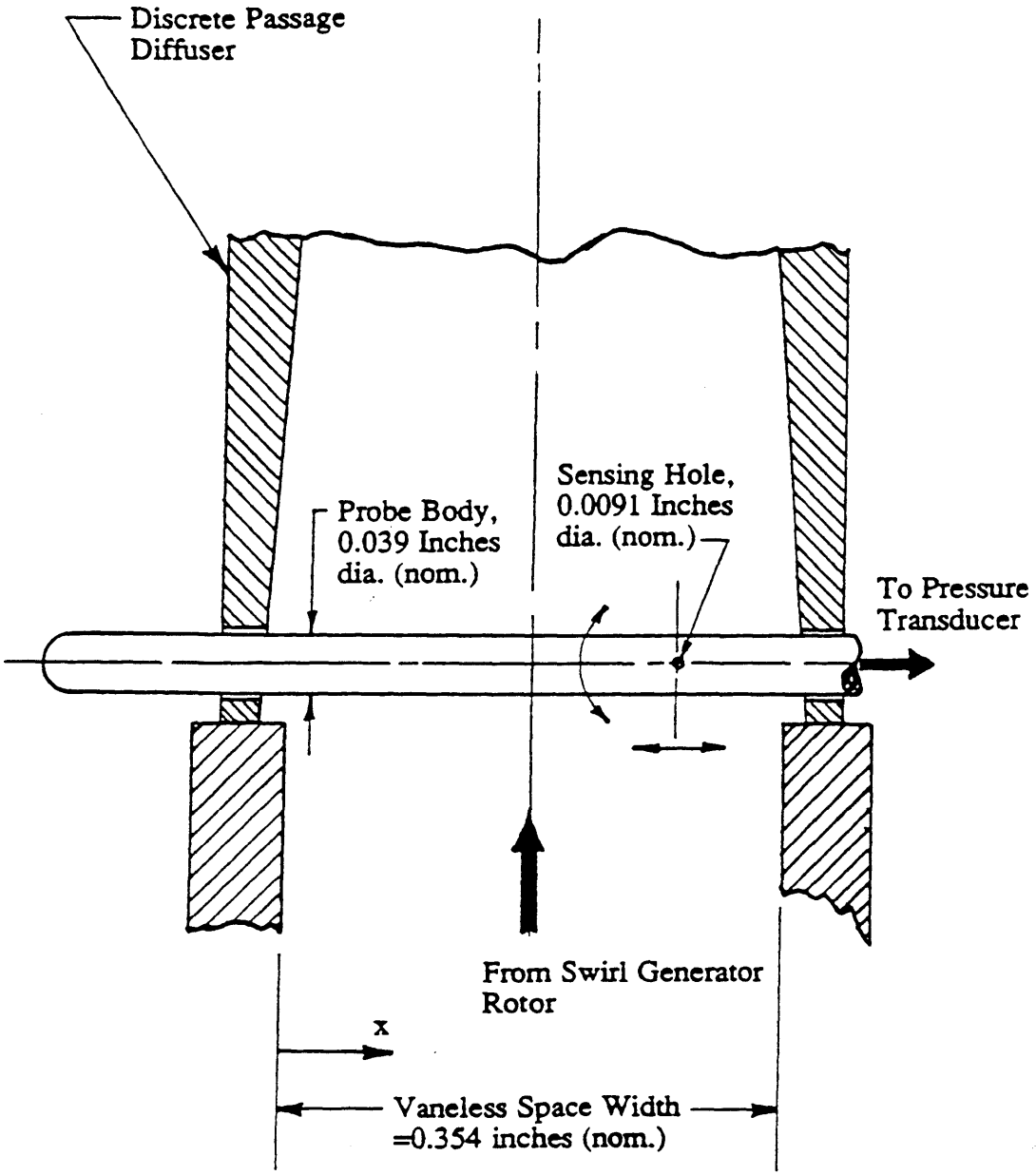

Figure 2.5: Traverse Probe Sketch [7].

Tap No.	ξ	ζ	Tap No.	ξ	ζ
1	0.779	0.059	16	3.058	0.0
2	1.250	0.0	17	3.211	0.0
3	1.659	-0.075	18	3.697	0.0
4	0.923	0.086	19	4.176	0.0
5	1.498	0.0	20	4.654	0.0
6	1.892	-0.085	21	5.142	0.0
7	1.75	0.117	22	5.621	0.0
8	1.745	0.0	23	6.200	0.0
9	2.134	-0.096	24	6.717	0.0
10	1.280	0.145	25	7.116	0.0
11	1.993	0.0	26	7.116	-0.335
12	2.450	-0.128	27	7.116	+.335
13	2.240	0.0	28	7.490	0.0
14	2.512	0.0	29	7.846	-0.350
15	2.785	0.0	30	8.172	-0.700

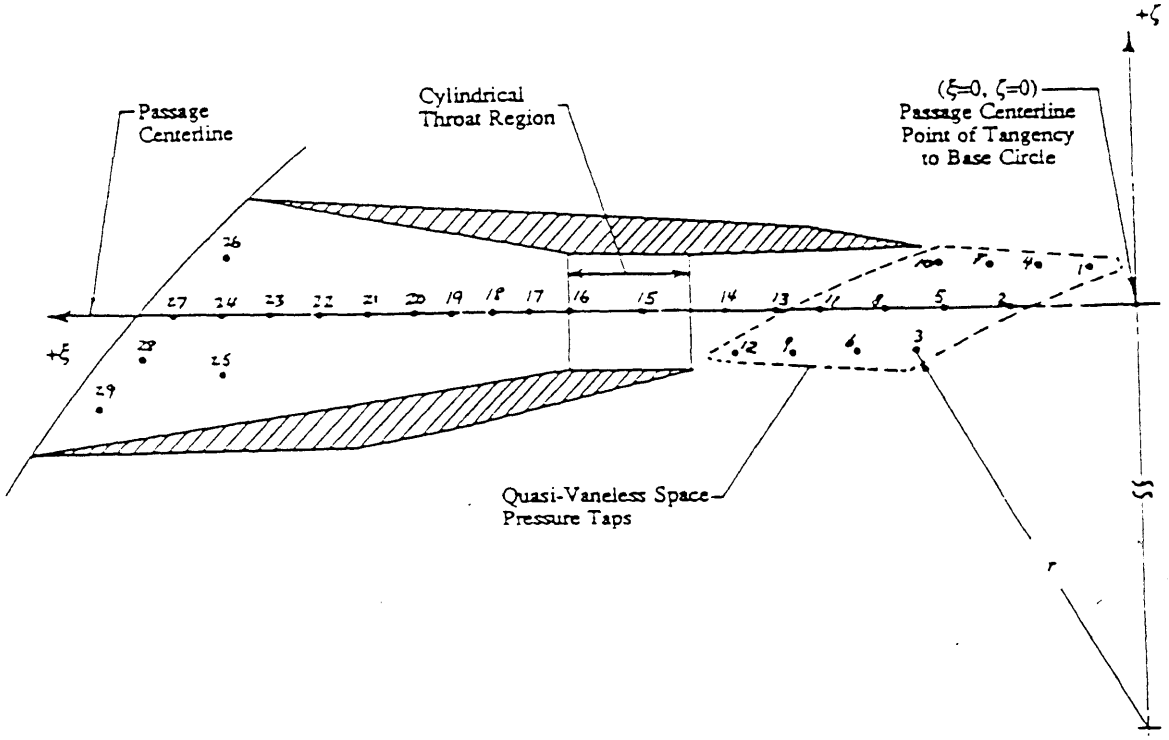

Figure 2.6: Passage #31 Static Tap Location Sketch for 30 Passage Pipe Diffuser [7].

Tap No.	ξ	ζ	Tap No.	ξ	ζ
1	0.803	0.057	18	3.268	0.0
2	1.023	0.083	19	3.393	0.0
3	1.314	0.102	20	3.850	0.0
4	1.544	0.134	21	4.300	0.0
5	1.250	0.0	22	4.750	0.0
6	1.540	0.0	23	5.210	0.0
7	1.837	0.0	24	5.660	0.0
8	1.637	-0.071	25	6.200	0.0
9	2.131	0.0	26	6.693	0.0
10	1.927	-0.084	27	7.186	0.0
11	2.424	0.0	28	7.186	0.0
12	2.218	-0.098	29	7.186	0.0
13	2.846	0.0	30	7.186	-0.275
14	2.519	-0.113	31	7.490	0.0
15	3.268	0.0	32	7.728	-0.230
16	3.268	0.0	33	7.952	-0.460
17	3.268	0.0			

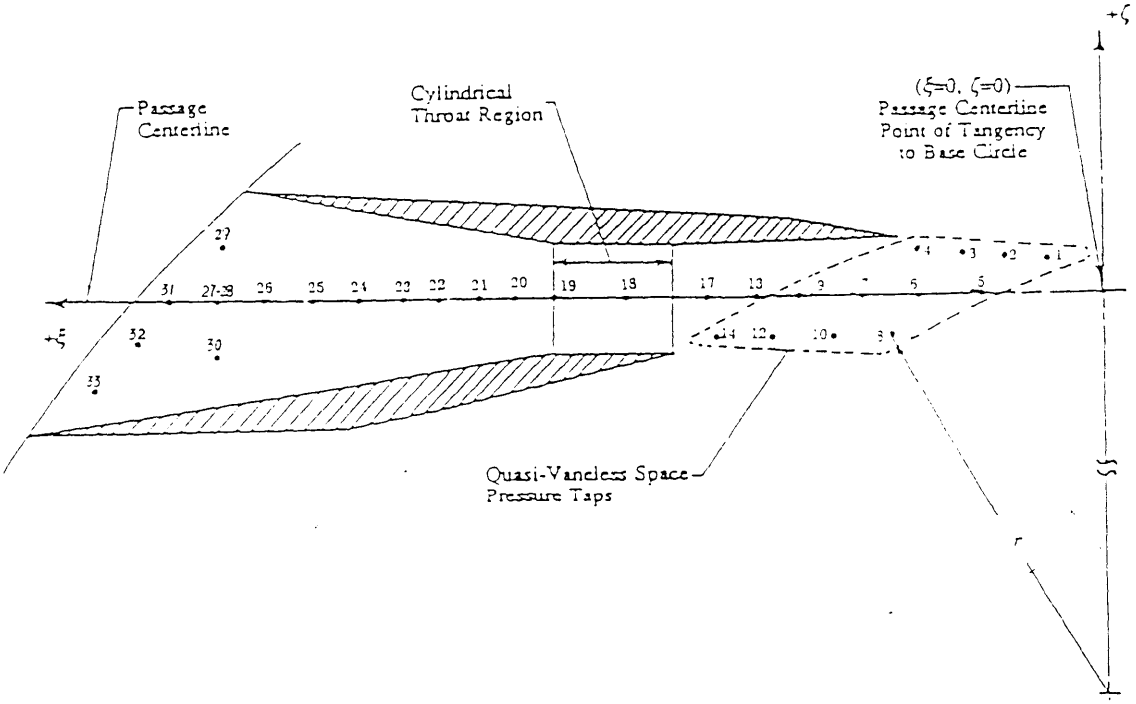

Figure 2.7: Passage #31 Static Tap Location Sketch for 38 Passage Pipe Diffuser

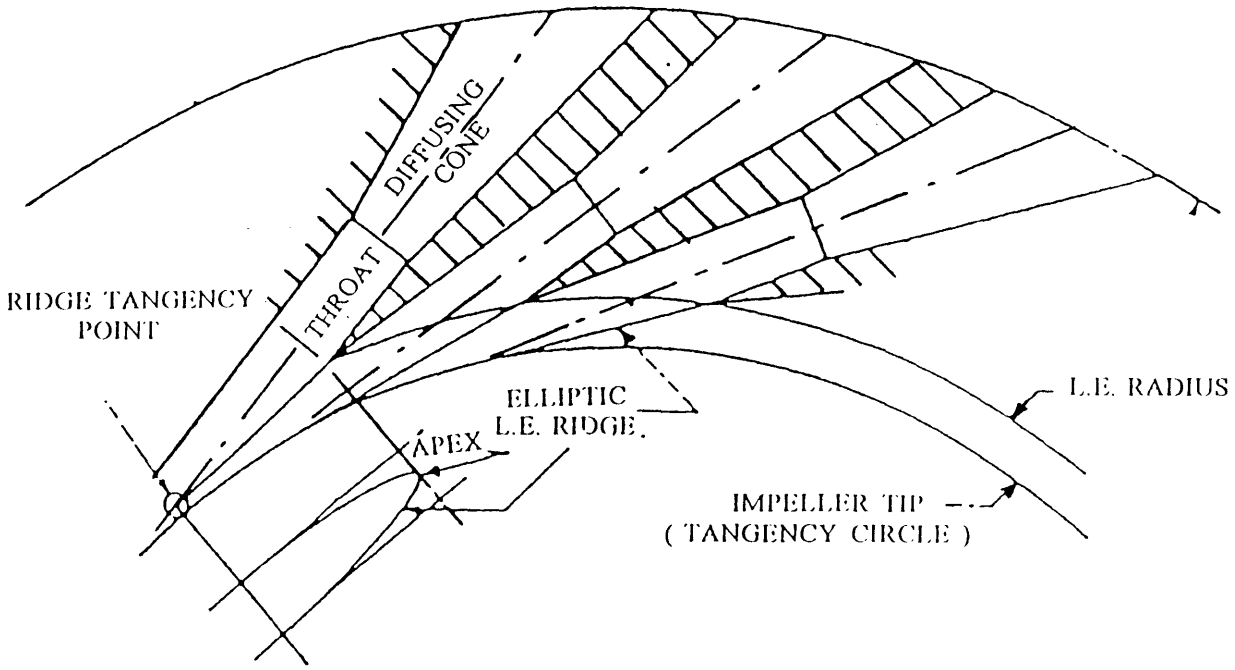

Figure 2.8: General Pipe Diffuser Geometry [4].

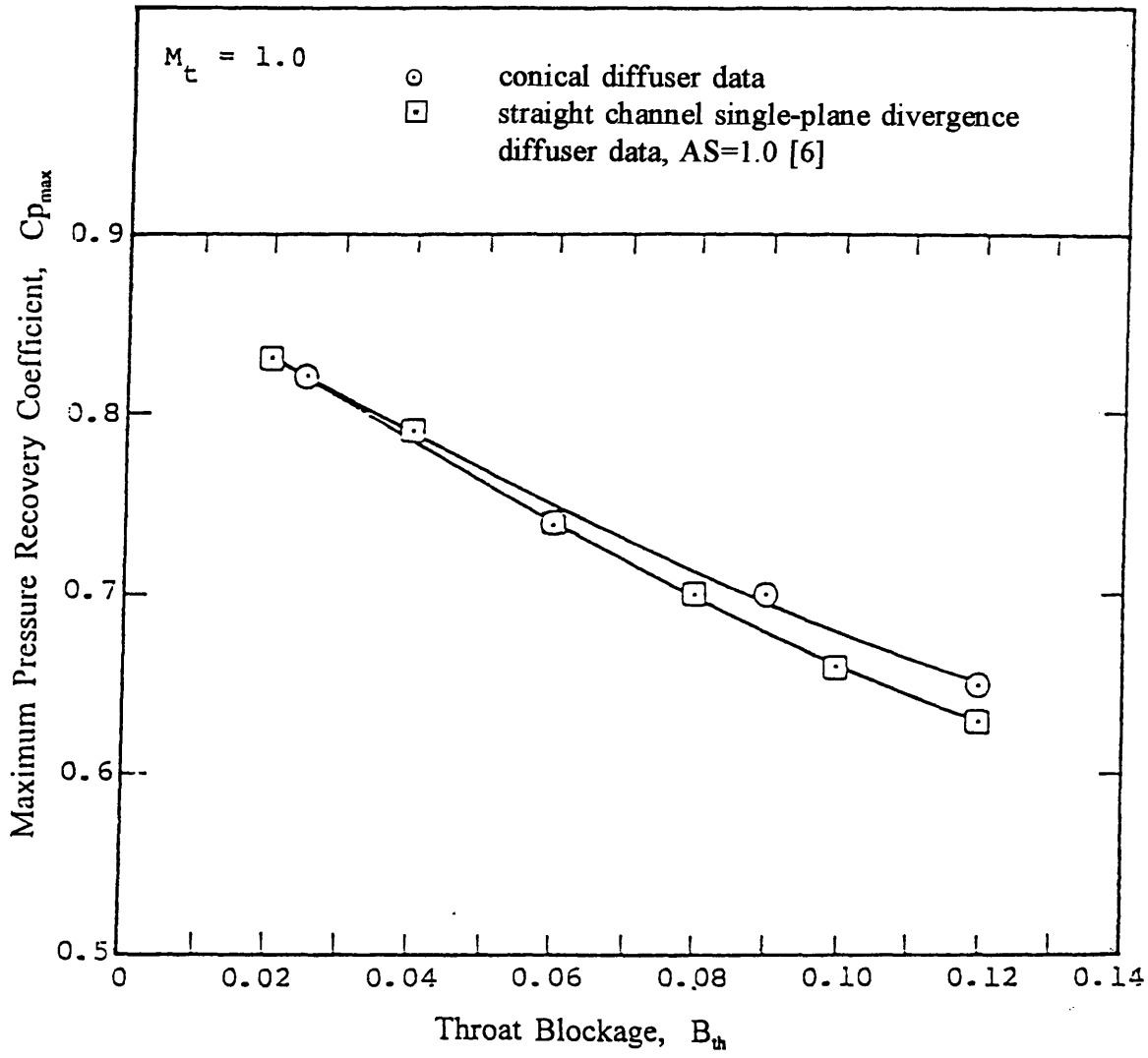

Figure 2.9: Maximum Pressure Recovery of Conical and Square Throat, Two Dimensional Diffusers [6].

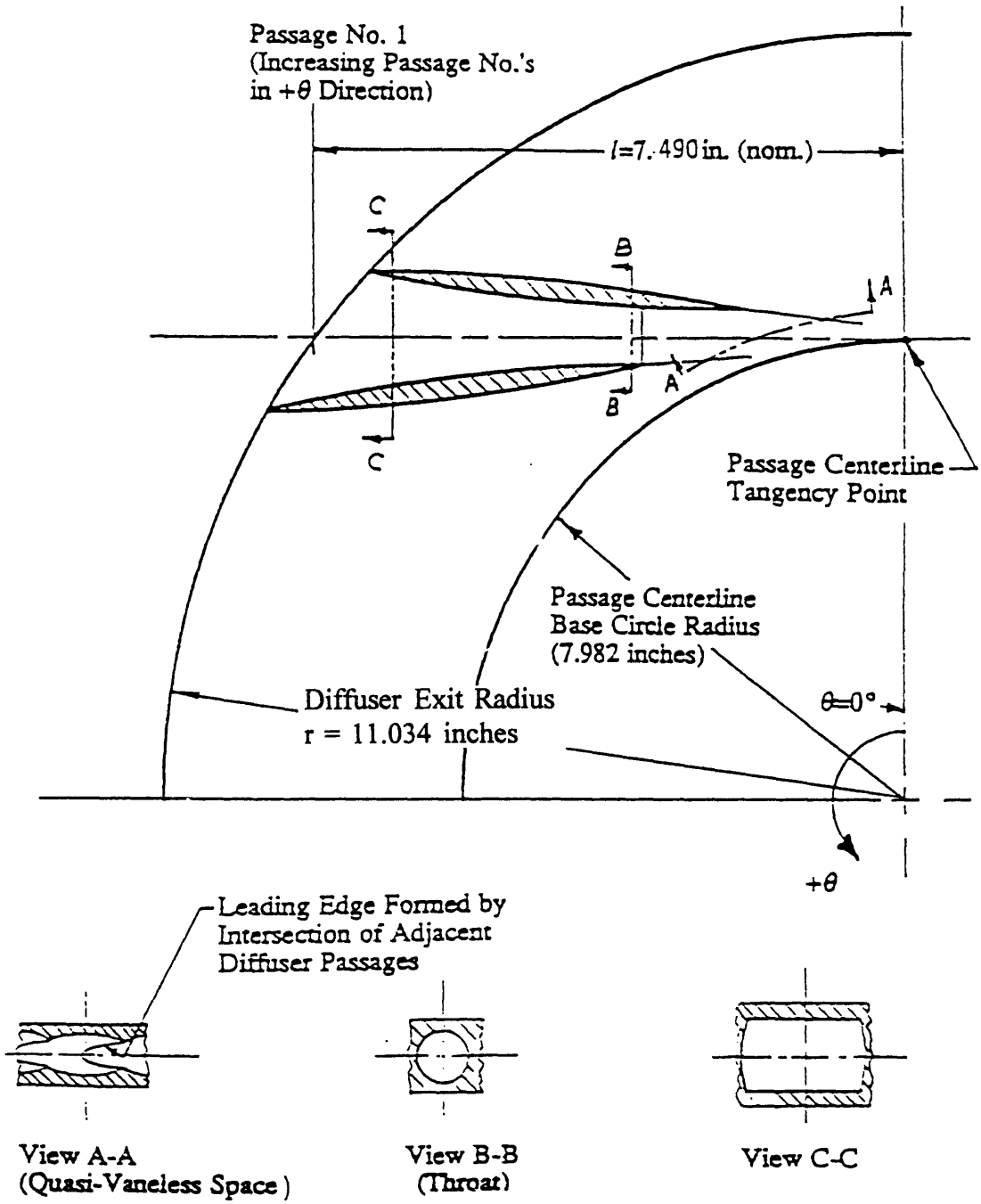

Figure 2.10: Discrete Passage Diffuser (38 Passage) Geometry Sketch [7].

Chapter 3

Performance Parameters

3.1 Operating Point Definition

We define the corrected mass flow and rotor speed as follows:

$$m_{corr} \equiv \frac{\sqrt{\frac{T_{amb}}{T_{ref}}}}{\frac{P_{amb}}{P_{ref}}} m_{actual} \qquad (3.1)$$

$$N_{corr} \equiv \frac{N_{act}}{\sqrt{\theta}} \qquad (3.2)$$

The parameter θ is defined as:

$$\theta = \frac{T_{t(inlet)}}{T_{ref}} \qquad (3.3)$$

The reference conditions are: P_{ref}= 14.7 (psi) and T_{ref} = 518.7 °R.

3.2 Total Temperature

Total temperature is measured in the plenum immediately downstream of the diffuser, equi-distance from aft and forward. We assume the flow process is adiabatic. The Mach number at the diffuser exit is less than 0.13 for rotor speed up to 6 KRPM for both 30 passage

and 38 passage diffuser, see Appendix E [7]. Because of this, no recovery correction was made to the total temperature measurement.

It is thus assumed that:

$$T_{t0}=T_{t1}=T_{t(1A)}=T_{t2}=T_{t(measured)} \qquad (3.4)$$

This treatment has been checked in the previous study [7] and proven satisfactory in the range of interest.

3.3 Mass Averaged Total Pressure and Total Pressure Availability

In addition to the availability averaged definition of total pressure, the mass averaged total pressure, conceptually simpler than the above, was also used by Filipenco. This is defined as:

$$\overline{P_{t1\,(mass)}}=\frac{\int_0^b P_{t1}\rho_1 V_{r1} 2\pi r_1 dx}{\int_0^b \rho_1 V_{r1} 2\pi r_1 dx} \qquad (3.5)$$

Figure 3.1 plots the difference between total pressure availability and mass averaged total pressure versus momentum averaged inlet flow swirl angle. This figure shows that there is little difference between the two different definitions. The differences are always less than 1% of the inlet dynamic pressure for the condition of interest.

3.4 Mass Averaged Angle and Momentum Averaged Angle

The mass averaged angle is defined as:

$$\overline{\alpha_{1\,(mass)}} = \frac{\int_0^b \alpha_1 \rho_1 V_{r1} 2\pi r_1 dx}{\int_0^b \rho_1 V_{r1} 2\pi r_1 dx} \qquad (3.6)$$

The momentum angle has been defined in the introduction chapter with Equation 1.5. Figure 3.2 plots mass Averaged angle versus momentum averaged angle. From the figure one can see that the two agree quite well and so the distinction between the two does not matter much. This result offer us the freedom to make the comparisons of results from different researchers even if they used different averaging method to compute the inlet swirl angle.

3.5 Static Pressure at Different Stations

For his experiments, Filipenco [7] used 4 static pressure probes at the radius of the traverse probe. He defined inlet static pressure as the average value of the four:

$$\overline{P_1} = \frac{1}{4} \sum_{n=1}^{4} P_{1_n} \qquad (3.7)$$

For the 38 passage diffuser experiments, Johnston [10] used 12 static pressure probes placed at radius of 8.20 inches to define the static pressure at that plane (he called it " 1A ") as the following:

$$\overline{P_{1A}} = \frac{1}{12} \sum_{n=1}^{12} P_{1A_n} \qquad (3.8)$$

Johnston described in detail how to obtain the static pressure at the inlet, where the radius is 8.001 inches, from the average static pressure

defined above.

The static pressure at the throat is defined as that in Equation 3.9 for the 38 passage diffuser, and that in Equation 3.10 for the 38 passage diffuser:

$$\overline{P_{th}} = \frac{1}{2}(P_{tap15} + P_{tap16}) \tag{3.9}$$

$$\overline{P_{th}} = \frac{1}{2}(P_{tap18} + P_{tap19}) \tag{3.10}$$

The static pressure definition at the diffuser exit is:
For the 30 passage diffuser:

$$\overline{P_2} = \frac{1}{4}(P_{tap26} + P_{tap27} + P_{tap28} + P_{tap29}) \tag{3.11}$$

For the 38 passage diffuser:

$$\overline{P_2} = \frac{1}{4}(P_{tap29} + P_{tap31} + P_{tap32} + P_{tap33}) \tag{3.12}$$

3.6 Inlet Blockage and Throat Blockage

Flow blockage is normally defined in the following two ways:

$$B = 1 - \frac{A_{(effective)}}{A_{(geometric)}} \tag{3.13}$$

for incompressible flow, and

$$B = 1 - \frac{m_{(actual)}}{m_{(ideal)}} \tag{3.14}$$

for compressible flow. In the present study, we used the latter to define

the blockages. The " actual " mass flow rate is the mass flow rate through the area of inlet measured by the venturi. The ideal mass flow rate is the rate if the flow had a uniform velocity distribution with the same total pressure and inlet static pressure.

The ideal mass flow rate is given as:

$$M_i = \sqrt{\frac{2}{k-1}\left[\left(\frac{P_{ti}}{P_i}\right)^{\frac{k-1}{k}} - 1\right]} \qquad (3.15)$$

$$m_{i\,(ideal)} = \left(\frac{P_{ti}}{RT_t}\right)\sqrt{kRT_t}M_i A_i \frac{1}{\left(1+\frac{k-1}{2}M_i^2\right)^{\frac{k+1}{2(k-1)}}} \qquad (3.16)$$

These formulas hold at the inlet and at the throat, with the subscript "i" referring to the location of interest. Blockages can be defined once we find the ideal mass at the inlet and throat via the above formulas.

3.7 Pressure Rise Coefficient at Different Stations

We define the overall pressure rise coefficient as:

$$Cp_{1-2} = \frac{P_2 - P_1}{\overline{P_{t1\,(mass)}} - P_1} \qquad (3.17)$$

Station 2 and station 1 stand for diffuser exit and inlet respectively. Instead of mass averaged total pressure, using total pressure availability defined in Equation 1.1, we get the following definition for the pressure rise coefficient as:

$$Cp_{1-2}^{\psi} = \frac{P_2 - P_1}{\overline{P_{t\psi 1}} - P_1} \qquad (3.18)$$

In this study, we also looked at the pressure at the different stations through the diffuser. One pressure rise coefficient is based on the pressure rise from the leading to the throat, and another is from the throat to the exit. The former is defined as:

$$Cp_{1-th} = \frac{P_{th} - P_1}{\overline{P_{t1\,(mass)}} - P_1} \qquad (3.19)$$

Where station " th" means the diffuser throat. The latter is defined as:

$$Cp_{th-2} = \frac{P_2 - P_{th}}{\overline{P_{tth\,(mass)}} - P_{th}} \qquad (3.20)$$

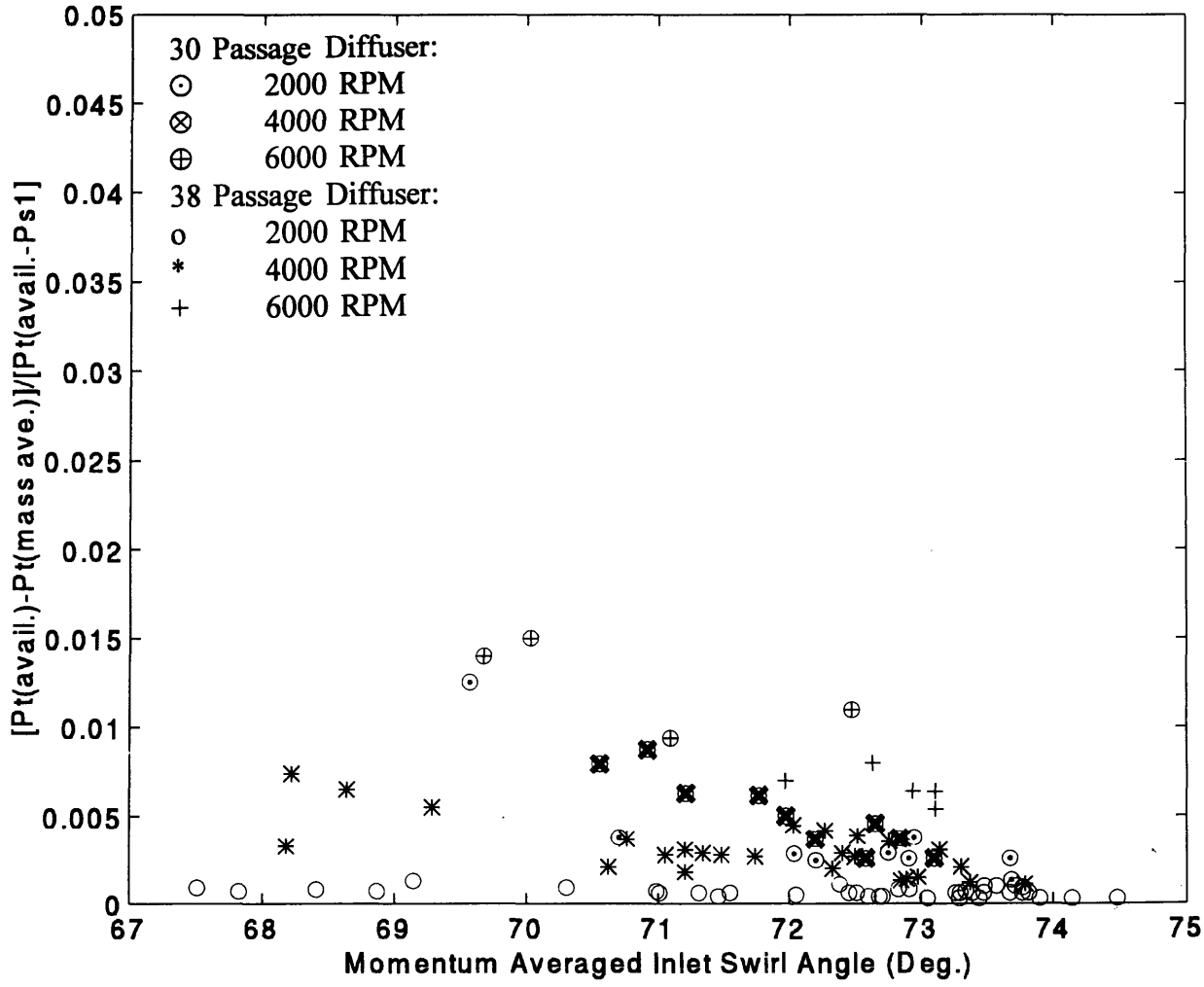

Figure 3.1: Difference between Mass Averaged Total Pressure and Total Pressure Availability.

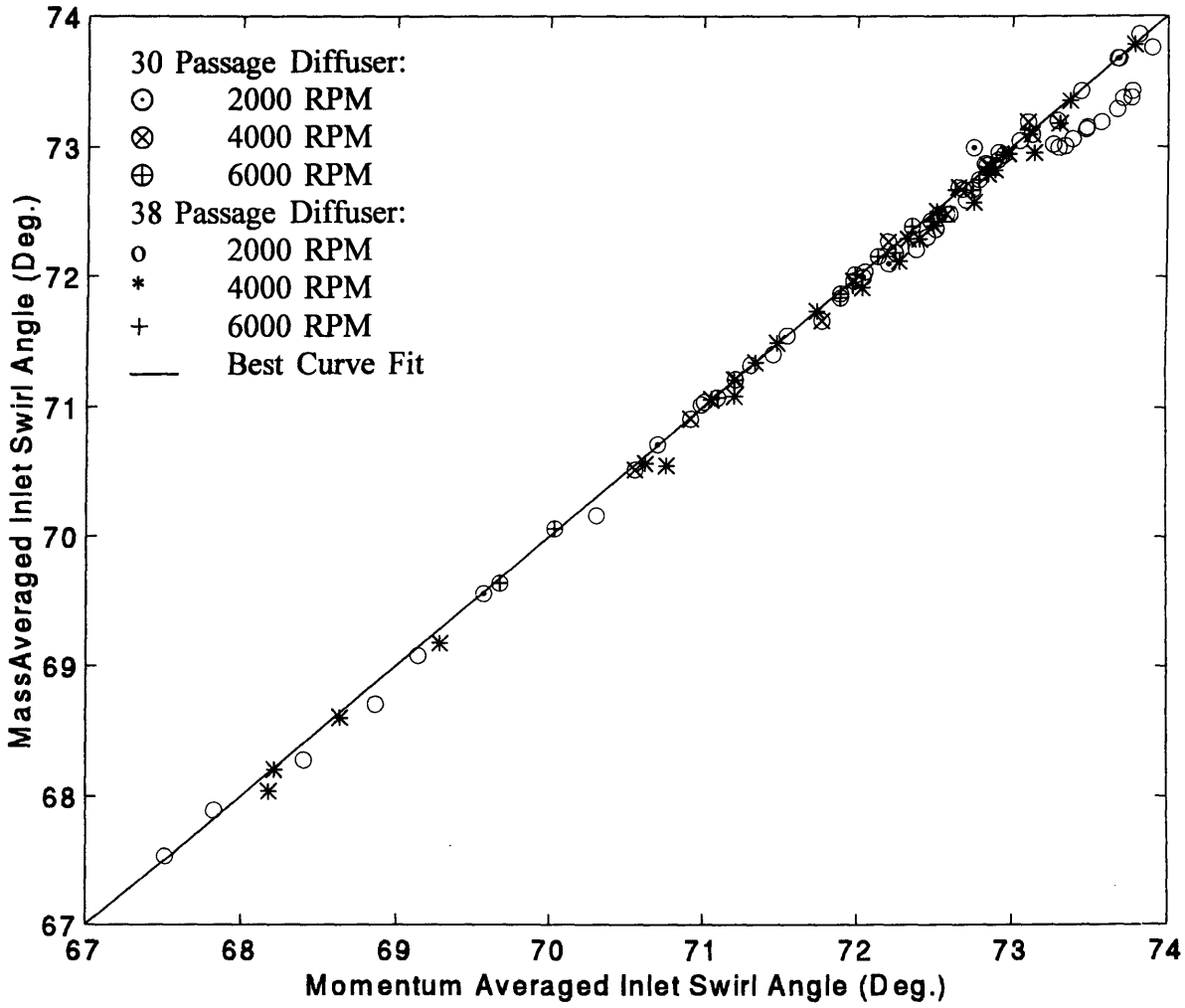

Figure 3.2: Comparison of Mass Averaged with Momentum Averaged Angle (Deg.).

Chapter 4

Summary of Data Examined

Two discrete passage diffuser have been tested in the swirl generator facility. The data can be summarized as in Table 4.1 and 4.2, steady data for 30 and 38 passages discrete passage diffuser; and in Table 4.3, unsteady data for the 38 passage diffuser. In both cases, the data were obtained at three pre-determined speeds: 2, 4, 6, KRPM. There are less valid data points for 30 passage diffuser.

Table 4.1 Steady Data for 30 Passage Discrete Passage Diffuser

	Rotor Speed	Data Set	Op.Point	Inlet Flow Condition
1	2000 RPM	119	119.1 119.2 119.3 119.4 119.5 119.6	Nominal
		162	162.2	
2	4000 RPM	122	122.3 122.4 122.6 122.8 122.9 122.10	
		125	125.4	
		126	126.1 126.2 126.3	
3	6000 RPM	123	123.2	
		127	127.3 127.4 127.5 127.6 127.8 127.9 127.10 127.11 127.12	
4	2000 RPM	155	155.2	Suction / Injection
		156	156.2 156.5	
5	4000 RPM	152	152.1 152.2	
		153	153.3	
		157	157.4 157.6	
6	6000 RPM	149	149.2 149.3	
		150	150.1 150.4	

Table 4.2 Steady Data for 38 Passage Discrete Passage Diffuser

Rotor speed		Data Set	Op.Point	Slot 3	Slot 4
2000 RPM	1	211	211.1-211.4; 211.6-211.12	Nominal	
	2	225	225.1-225.10	Suction	
	3	226	226.1 226.2 226.3 226.5		Suction
	4	227	227.1 227.2 227.4	Suction	
	5	228	228.3 - 228.6	Injection	
	6	229	229.1 229.2 229.3		Injection
	7	230	230.1-230.4	Injection	
	8	231	231.1-231.3	Suction	Injection
	9	232	232.1-232.3	Injection	Suction
4000 RPM	10	215	215.1-215.3 215.6-215.8 215.9 215.10	Nominal	
	11	233	233.1-233.4	Suction	
	12	234	234.1 234.2 234.4 234.6		Suction
	13	235	235.2 235.3	Suction	
	14	237	237.2-237.6	Injection	
	15	238	238.1 238.2 238.3		Injection
	16	239	239.1 239.2	Injection	
	17	240	240.2 240.3 240.4	Suction	Injection
	18	241	241.1 241.2 241.3	Injection	Suction
6000 RPM	19	249	249.2 249.5 249.7 249.8 249.9 249.10	Nominal	
	20	255	255.2	Suction	

Table 4.3 Unsteady Data for 38 Passage Discrete Passage Diffuser

Rotor Speed		Data Set	Op.point	
2000 RPM	1	214	214.1 214.2 214.3	With Probe
	2	221	221.1 - 221.8	
	3	222	222.1 - 222.3	
	4	245	245.1 - 245.3	
4000 RPM	5	216	216.1 - 216.3	
	6	217	217.1 - 217.10	
	7	223	223.1 - 223.9	
	8	224	224.1 - 224.6	
	9	242	242.1 - 242.3	
	10	244	244.1 - 244.3	
	11	246	246.1 246.2	
	12	247	247.1 - 247.6	
	13	248	248.1 - 248.4	
	14	256	256.1 - 256.8	Without Probe
	15	257	257.1 257.2	
	16	258	258.1	
6000 RPM	17	250	250.1 - 250.4	With Probe

Chapter 5
Results

5.1 Range of Inlet Conditions

For the two discrete passage diffusers, thirty one combinations of Mach numbers and diffuser inlet flow profiles were available. Figure 5.1 shows the range of momentum averaged inlet angle and inlet blockage, as defined in Equations 1.5 and 3.14 respectively, for both diffusers, the former ranges from 67.0 to 74.8 degrees, and the latter from 0.02 to 0.19. The figure shows little correlation between inlet blockage and inlet swirl angle, indicating that the flow profile modifiers are effective in controlling the inlet flow distribution.

5.2 Diffuser Pressure Rise Characteristic

5.2.1 Overall Pressure Rise versus Inlet Blockage

Inlet blockage is generally considered to be an important factor in determining static pressure performance for a straight channel diffuser. The pressure rise of such diffusers decreases when inlet blockage is increased. Figure 5.2 plots diffuser static pressure rise coefficient as defined in Equation 3.18 versus inlet blockage for the two discrete passage diffusers. The figure shows little correlation between the inlet blockage and the overall pressure rise coefficient. The geometrical difference between a straight channel diffuser and a discrete passage diffuser is that the former does not have an entry region, the region from the leading edge to the throat, whereas the latter does. One can thus ask whether the difference between the pressure rise performance of a straight

channel diffuser and a discrete passage diffuser can be attributed to the entry region of the discrete passage diffuser.

Filipenco [7] showed that if one used the proper variables, changes in inlet distortion parameters characterizing the mass, momentum, kinetic energy and skew non-uniformities have no significant effect on the static pressure rise of the diffuser. His conclusion was that for a given momentum averaged swirl angle, the static pressure rise coefficient, as defined in Equation 3.18 is essentially independent of inlet conditions. The approach taken to investigate the prime parameter(s) in determining the static pressure rise coefficient is to look at how, and why, the inlet swirl angle has such a role.

5.2.2 Overall Pressure Rise versus Momentum Averaged inlet Angle

Figure 5.3 presents the overall diffuser static pressure rise coefficient versus momentum averaged inlet swirl angle. The figure shows an approximately linear relation between these two parameters. In addition, both diffusers are seen to exhibit similar trends. To see how the relation between inlet swirl angle and pressure rise coefficient comes about, we need to consider throat blockage and effective area ratio of inlet to throat.

Figure 5.4 shows how the geometric area ratio and effective area ratio change with inlet swirl angle. The former is defined in Equation 5.3, and the latter is defined as the following:

$$AR_{effective}=\frac{A_{th}(1-B_{th})}{A_1(1-B_1)} \qquad (5.1)$$

Definition of blockage has been given in Equation 3.14. Figure 5.4 shows that the effective area ratio is consistently larger than the geometric area ratio. There is a decrease in blockages from the inlet to the throat which makes the corresponding ideal pressure rise coefficient larger. In other words the actual pressure rise in the diffuser is less efficient than that based on geometrical area.

5.2.3 Pressure Rise Coefficient Before Throat versus Inlet Conditions

The inlet flow parameters which can affect the pressure rise coefficient before the throat are inlet blockage, momentum averaged inlet swirl angle, Mach number and incidence. We introduce the ideal Cp, which is defined for the case of lossless flow:

$$Cp_{ideal}=\frac{P_{th}-P_1}{\frac{1}{2}\rho U_1^2} \qquad (5.2a)$$

For incompressible flow:

$$Cp_{ideal}=1-\frac{1}{AR^2} \qquad (5.2b)$$

where

$$AR=\frac{A_{th}}{A_1} \qquad (5.3)$$

Subscripts "1" and "th" refer to inlet and throat respectively. In Equation 5.3, A_{th} and A_1 are the geometric areas of the throat and inlet.

The definition for actual pressure rise before the throat is:

$$Cp_{1\text{-}th} = \frac{P_{th} - P_1}{P_{t\psi 1} - P_1} \qquad (5.4)$$

where the total pressure availability has been defined before in Equation 1.1.

Figure 5.5 presents the $Cp_{1\text{-}th}$ as defined in Equation 5.4 versus inlet blockag. There is no obvious relationship between static pressure rise coefficient and inlet blockage. Figure 5.6 shows $Cp_{1\text{-}th}$ versus momentum averaged inlet swirl angle. This pressure rise coefficient does have a dependence on the momentum averaged inlet swirl angle. The trend for the 30 passage diffuser is slightly higher than that for the 38 passage diffuser, but the difference does not suggest they don't have the same trend. We can also plot Cp_{ideal} versus Cp_{actual} to see how well they agree, which is shown in Figure 5.7 and the bestfit of the two diffuser data obviously agree with the ideal value well. A similar result was also obtained by Hunziker [14], shown in Figure 5.8. The figure presents data obtained at three different inlet Mach number: 0.40, 0.60, 0.75. From this one can see the pressure rise coefficient does not depend on inlet Mach number over this range, but is mainly determined by the area ratio, which is a function of inlet swirl angle.

The actual Cp should be less than the ideal Cp, but the data presented do not show this. One reason for this can be that the blockage at the inlet and the throat is different and that the blockage has actually decreased. This will be explored below.

5.2.4 Throat Total Pressure and Throat Blockage

It is often assumed that throat total pressure is the same as inlet

total pressure. We now examine how good this approximation is.

At the throat, we measure static pressure P_{th}, mass flow rate m, area A_{th}, and stagnation temperature T_0. We have the following three equations:

$$m_{th\,(ideal)} = \left(\frac{P_{tth}}{RT_t}\right)\sqrt{kRT_t}M_{th}A_{th}\frac{1}{\left(1+\frac{k-1}{2}M_{th}^2\right)^{\frac{k+1}{2(k-1)}}} \qquad (5.5)$$

$$\frac{P_{tth}}{P_{th}} = \left(1+\frac{k-1}{2}M_{th}^2\right)^{\frac{k}{(k-1)}} \qquad (5.6)$$

$$B_{th} = 1 - \frac{m_{th}}{m_{th\,(ideal)}} \qquad (5.7)$$

There are four unknowns to be determined: $m_{th(ideal)}$, P_{tth}, M_{th}, B_{th}.

An empirical relation between throat blockage and static pressure rise coefficient ($Cp_{1\text{-}th}$)from leading edge to throat, was given by Kenny [3], based on data from various diffuser geometries. Figure 5.9 shows Kenny's result for throat blockage versus static pressure rise coefficient from diffuser leading edge to throat [3]. Both pipe diffusers and vaned diffusers have a correlation between throat blockage and pressure rise coefficient from diffuser leading edge to diffuser throat. Figure 5.10 is a curve fit of Kenny's experimental data for pipe diffusers with leading Mach number less than unity. The curve fit has the following form:

$$B_{th} = .1144Cp_{1\text{-}th}^4 + .2194Cp_{1\text{-}th}^3 + .1600Cp_{1\text{-}th}^2 + .0663Cp_{1\text{-}th} + .0414 \qquad (5.8)$$

Because we know how $Cp_{1\text{-}th}$ varies with momentum averaged inlet swirl angle, Equation 5.8 allows us to link the throat blockage to the inlet swirl

angle as well.

Figure 5.11 thus shows the relation between throat blockage and momentum averaged inlet swirl angle. The static pressure rise coefficient $Cp_{1\text{-}th}$ is an approximately linear function of momentum averaged inlet swirl angle, so a similar shape of Figures 5.10 and 5.11 is expected. As mixing increases in the entry region of diffuser, blockage will decrease. Since the throat blockage depends only on the momentum averaged inlet swirl angle, that angle must determine the amount of mixing. More mixing occurs at smaller inlet flow angle, which results in lower blockage at the throat, but larger loss of total pressure in this region.

Figure 5.12 presents the pressure rise coefficient $Cp_{1\text{-}th}$, from leading edge to throat, versus inlet swirl angle. The inlet blockage and the throat blockage are included in the calculation of area ratio of streamtube of throat over inlet, as defined in Equation 5.1. This figure shows that the actual pressure rise coefficient is smaller than the ideal value, for incompressible, lossless flow.

5.2.5 Total Pressure Loss from the Leading Edge to the Throat

We can also calculate the total pressure loss from the leading edge to the throat. The procedure for doing this is given in Appendix A. Figure 5.13 shows the total pressure loss $\Delta P_{t(1\text{-}th)}/(1/2\rho V^2_{(inlet)})$, from the leading edge to the throat, as a function of momentum averaged inlet swirl angle. It shows that the total pressure loss ahead of the throat is substantial, especially at smaller inlet swirl angle.

Figure 5.14 shows how $\Delta P_{t(1\text{-}th)}/(1/2\rho V^2_{(inlet)})$ and throat blockage are related. More total pressure loss inside the entry region is incurred when the throat blockage is smaller. A suggested explanation is that with the

same inlet blockage, more mixing occurs to lower the blockage at the throat for the case with smaller throat blockage, resulting in more mixing loss from leading edge to throat.

5.2.6 Pressure Rise after Throat versus Throat Blockage

The static pressure rise coefficient for the channel part of a vaned diffuser is generally defined as [8]:

$$Cp'_{th-2} = \frac{P_2 - P_{th}}{\overline{P_{t1}^{mass}} - P_{th}} \qquad (5.9)$$

In Equation 5.9, P_2 and P_{th} are the static pressures of the exit and throat, and the total pressure at the throat is assumed to be equal to the inlet total pressure.

Figure 5.15 [8] shows that the pressure rise coefficient as defined in this manner is constant or increases slightly as throat blockage increases. Figure 5.16 is the pressure rise coefficient Cp'_{th-2} for the two discrete passage diffusers. The trend shown does not conform to that of a conventional two dimensional diffuser and we can inquire whether the channel part of a discrete passage diffuser (or vaned diffuser) has a behavior similar to a two dimensional diffuser.

Figure 5.16 is based on using inlet total pressure as throat total pressure. The computed total pressure at the throat, however, is quite different. If we use this computed total pressure, we can define the static pressure rise for the channel part of the discrete passage diffuser, ie, the part from the throat to the exit of the diffuser, as follows:

$$Cp_{th-2} = \frac{P_2 - P_{th}}{P_{tth} - P_{th}} \qquad (5.10)$$

Figure 5.17, which gives Cp_{th-2} versus throat blockage, shows that the trend of the results agrees well with that of the two dimensional diffuser data. When throat blockage increases, static pressure rise coefficient decreases. The definition in Equation 5.10, which uses the computed throat total pressure rather than the total pressure at the inlet for the definition of pressure rise coefficient, is thus the more appropriate one.

5.3 Predicting the Pressure Rise Coefficient of a Discrete Passage Diffuser

The previous section showed that the channel of a discrete passage diffuser behaves similar to a two dimensional diffuser if we use the correct characteristic parameters. Neglecting the total pressure loss inside the entry region can lead to the result that the channel pressure rise coefficient can vary with throat blockage in an incorrect manner. To properly interpret the performance of a diffuser, one needs to find the total pressure loss inside the entry region.

With different geometries, the geometrical area ratio, A_{th}/A_1 will vary differently with the inlet swirl angle. Figure 5.18 shows how this area ratio varies with inlet swirl angle with different inlet radius but same throat area. We can see that the geometrical area ratio varies differently with different inlet radius. The ideal pressure rise coefficient,

corresponding to this, is given in Figure 5.19. Actual pressure rise coefficient data from leading edge to throat for the two diffusers are also plotted with best curve fit in this figure. This figure shows the actual pressure rise coefficient data agree well with its ideal value corresponding to the geometry with the inlet radius of 8.0 inches. Since the ideal pressure rise coefficient versus inlet swirl angle for different inlet radius is different and the actual pressure rise coefficient versus inlet swirl angle is close to its corresponding ideal value, therefore the actual pressure rise coefficient versus inlet swirl angle is different for each different radius and it can be approximated by the corresponding ideal value.

Based on the above ideas, a procedure to predict the static pressure rise of a diffuser with given inlet condition (total pressure, static pressure, mass flow rate, inlet swirl angle) can be developed as follows.

1) From the inlet swirl angle α, calculate the area ratio A_{th}/A_1, and $Cp_{1\text{-}th}$. Then, using Equation 3.19, we can compute the static pressure at the throat P_{th}.

2) From $Cp_{1\text{-}th}$ estimate the throat blockage using Equation 5.8.

3) Using throat blockage, calculate the total pressure loss inside the entry region, and therefore the total pressure at the throat.

4) Use B_{th} to find $Cp_{th\text{-}2}$ from two dimensional diffuser data.

5) Using the results obtained in 1), 3), 4), find the static pressure rise from inlet to exit.

The flow chart of the procedure to predict the pressure rise coefficient of a discrete passage diffuser can be found in Appendix B.

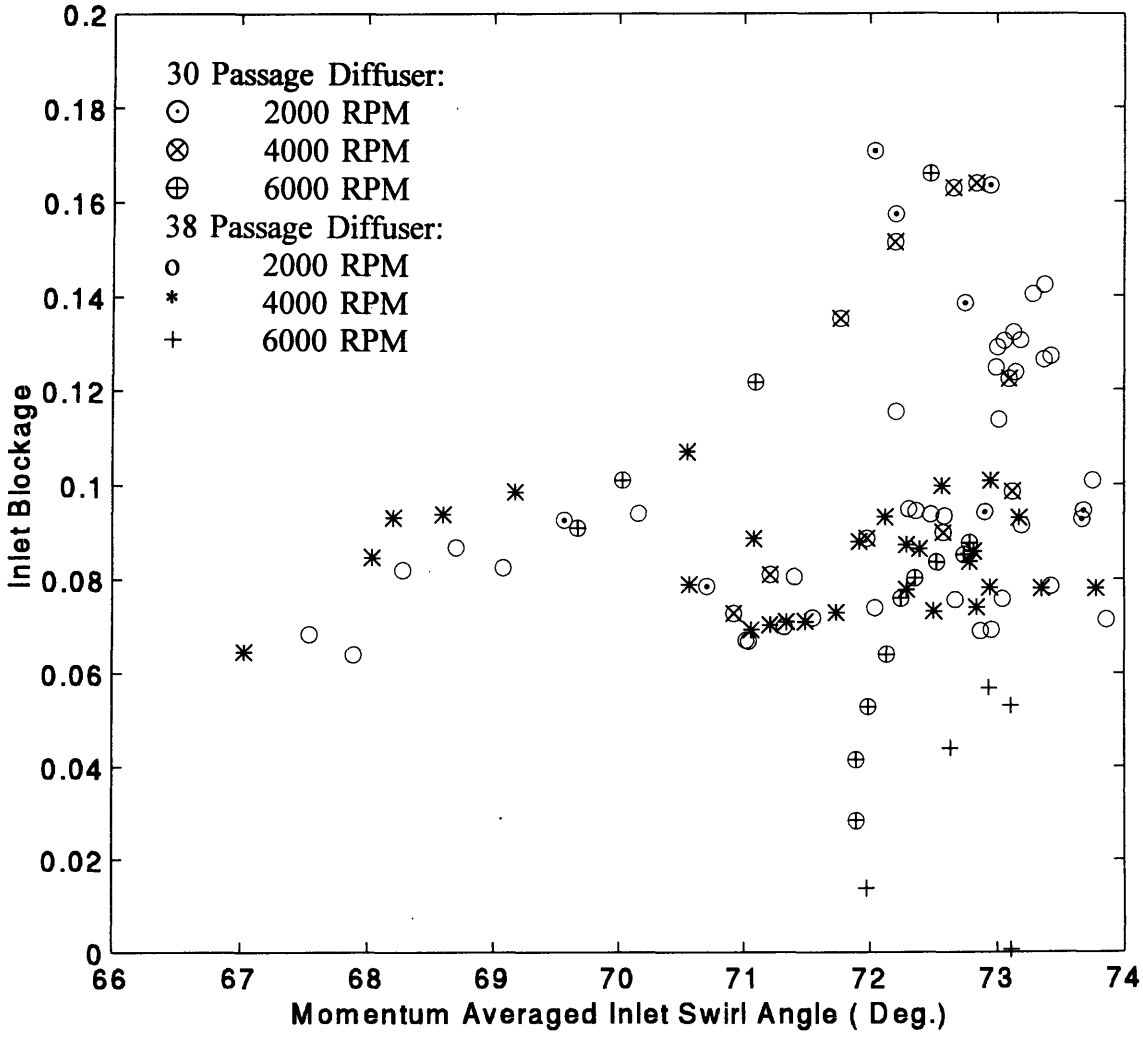

Figure 5.1: Ranges of Inlet Flow Angle (Deg.) and Inlet Blockage for two Discrete Passage Diffusers.

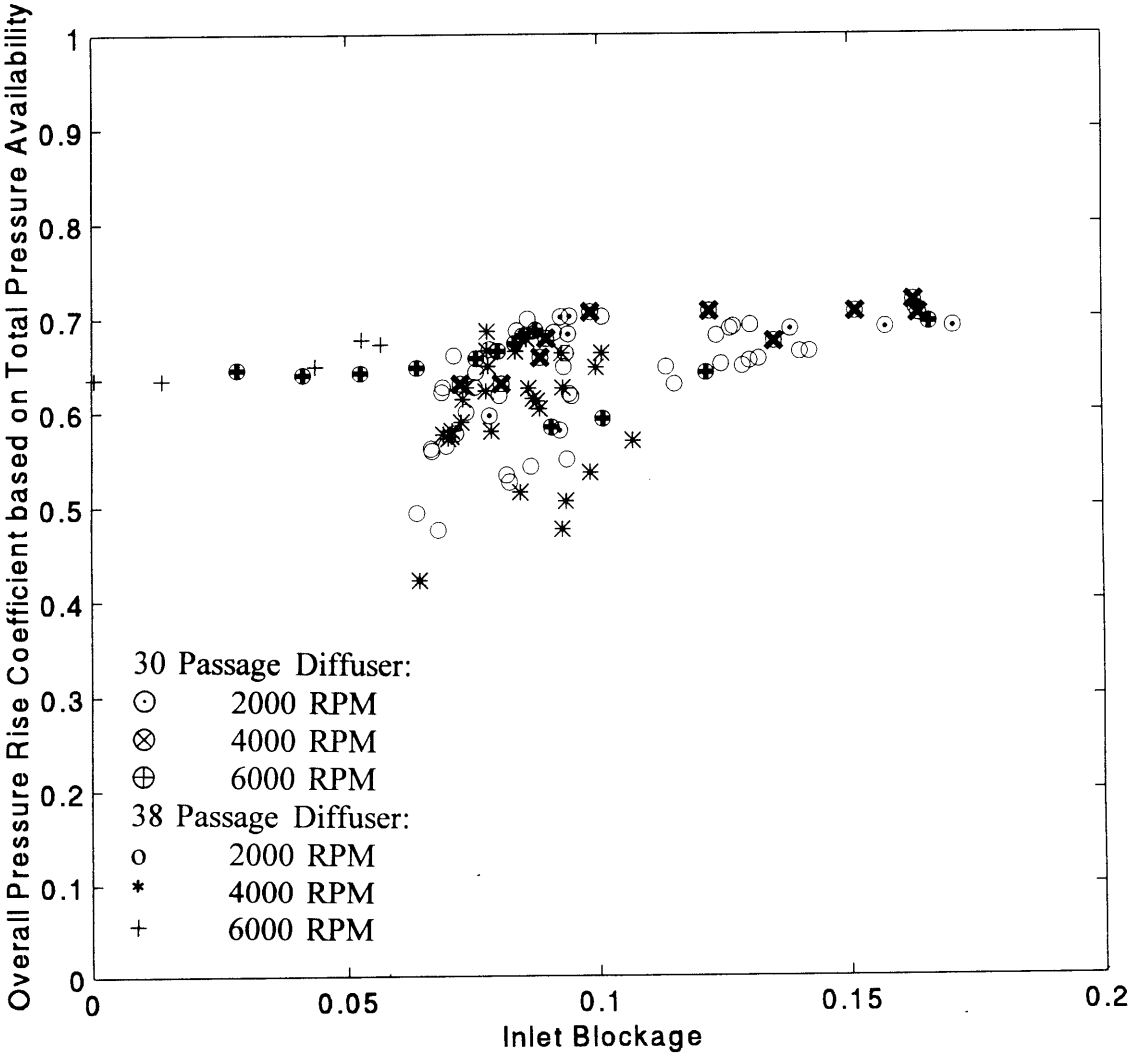

Figure 5.2: Overall Pressure Rise versus Inlet Blockage for the two Discrete Passage Diffusers.

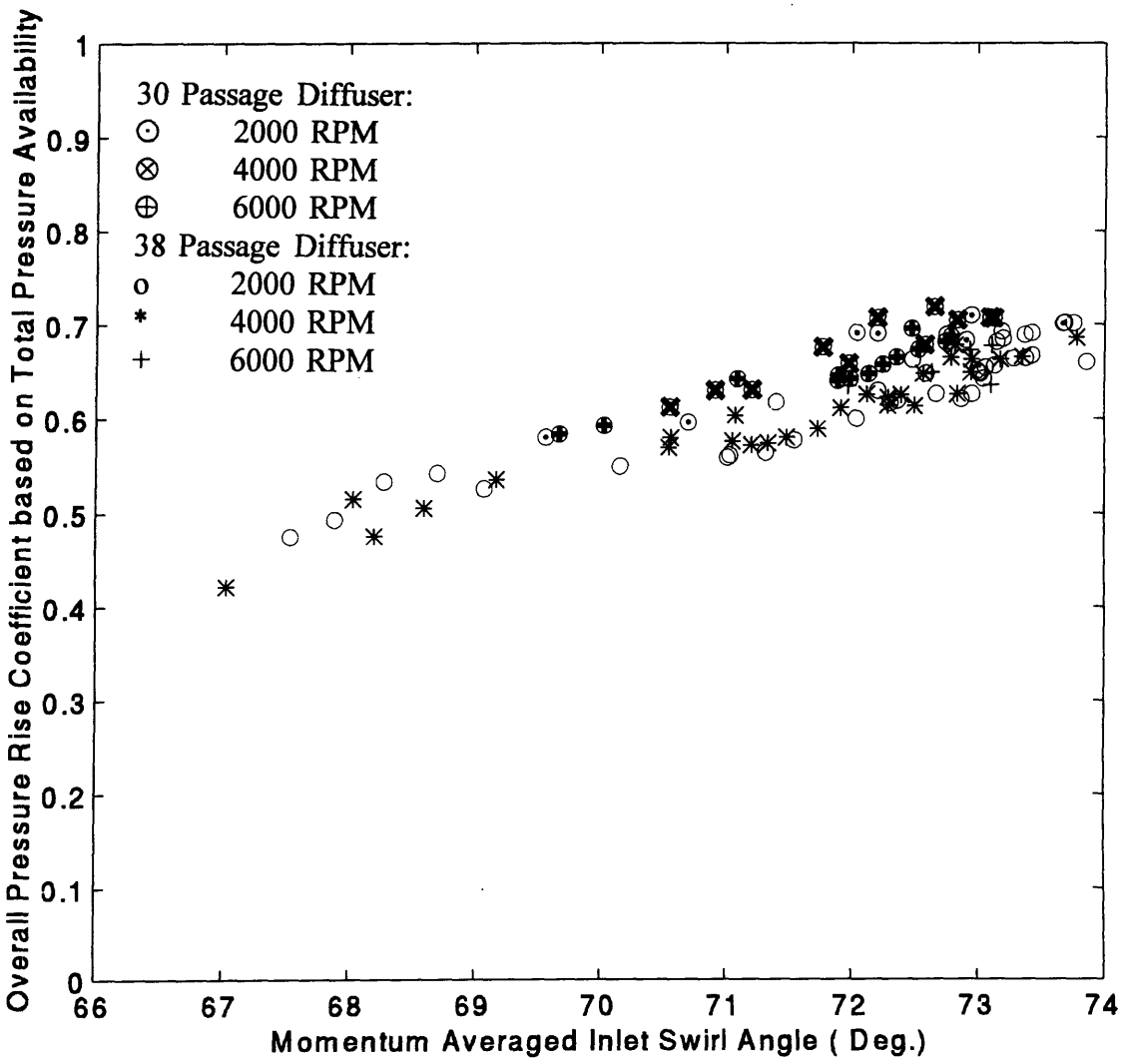

Figure 5.3: Overall Pressure Rise Coefficient versus Inlet Swirl Angle for th two Discrete Passage Diffusers.

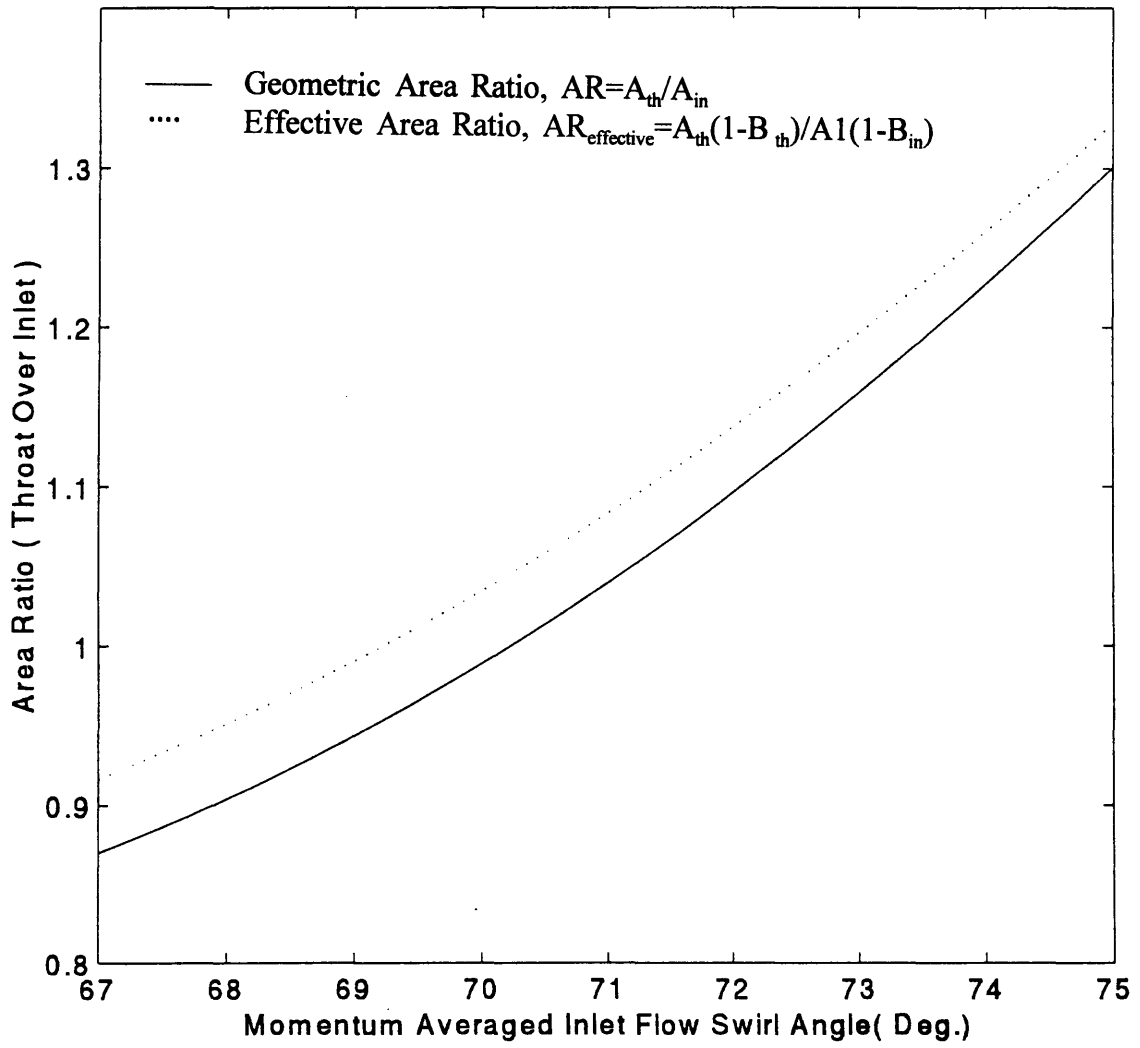

Figure 5.4: Area Ratio of Throat over Inlet Flow Streamtube.

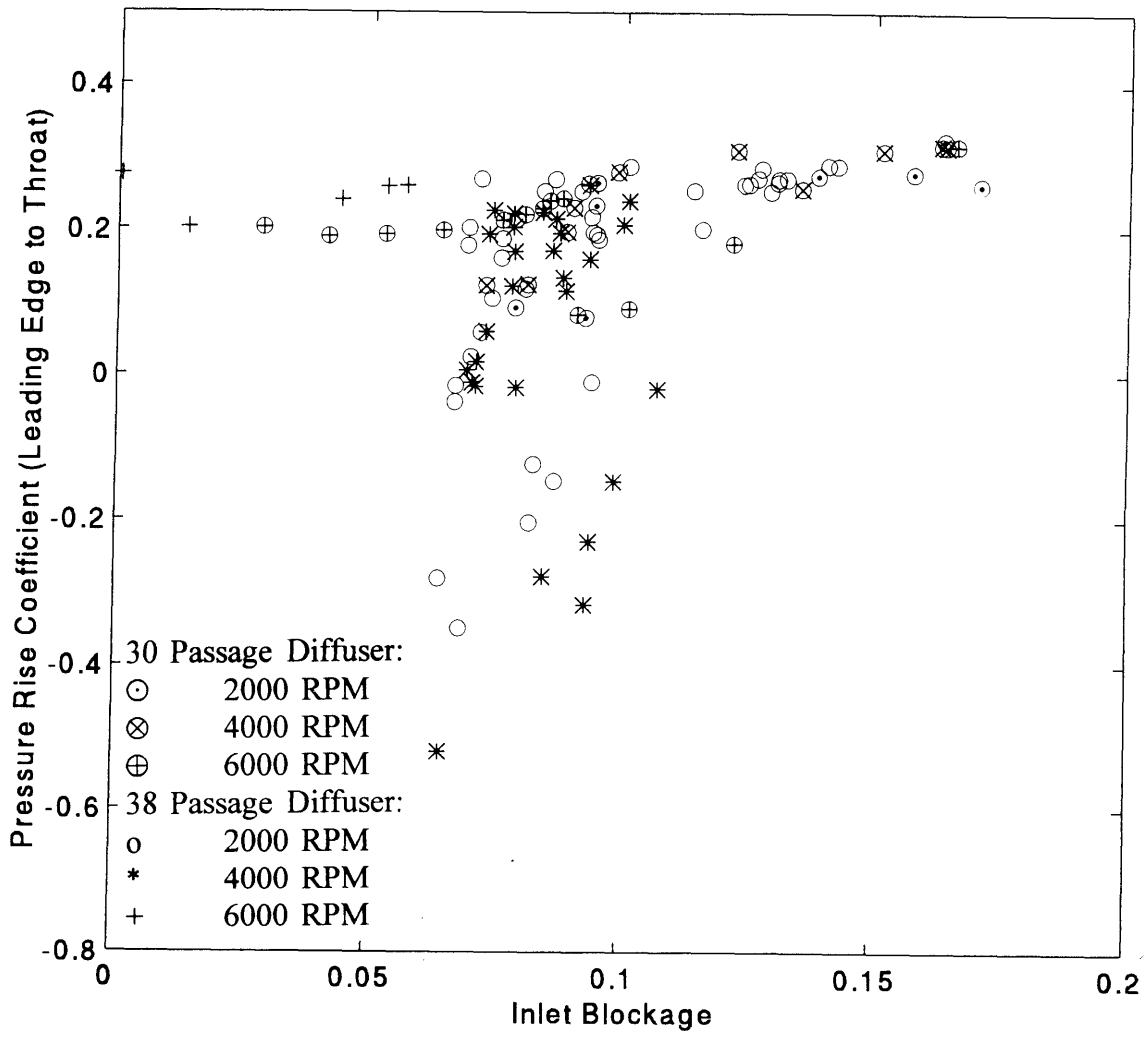

Figure 5.5: Static Pressure Rise Coefficient from Leading Edge to Throat versus Inlet Blockage.

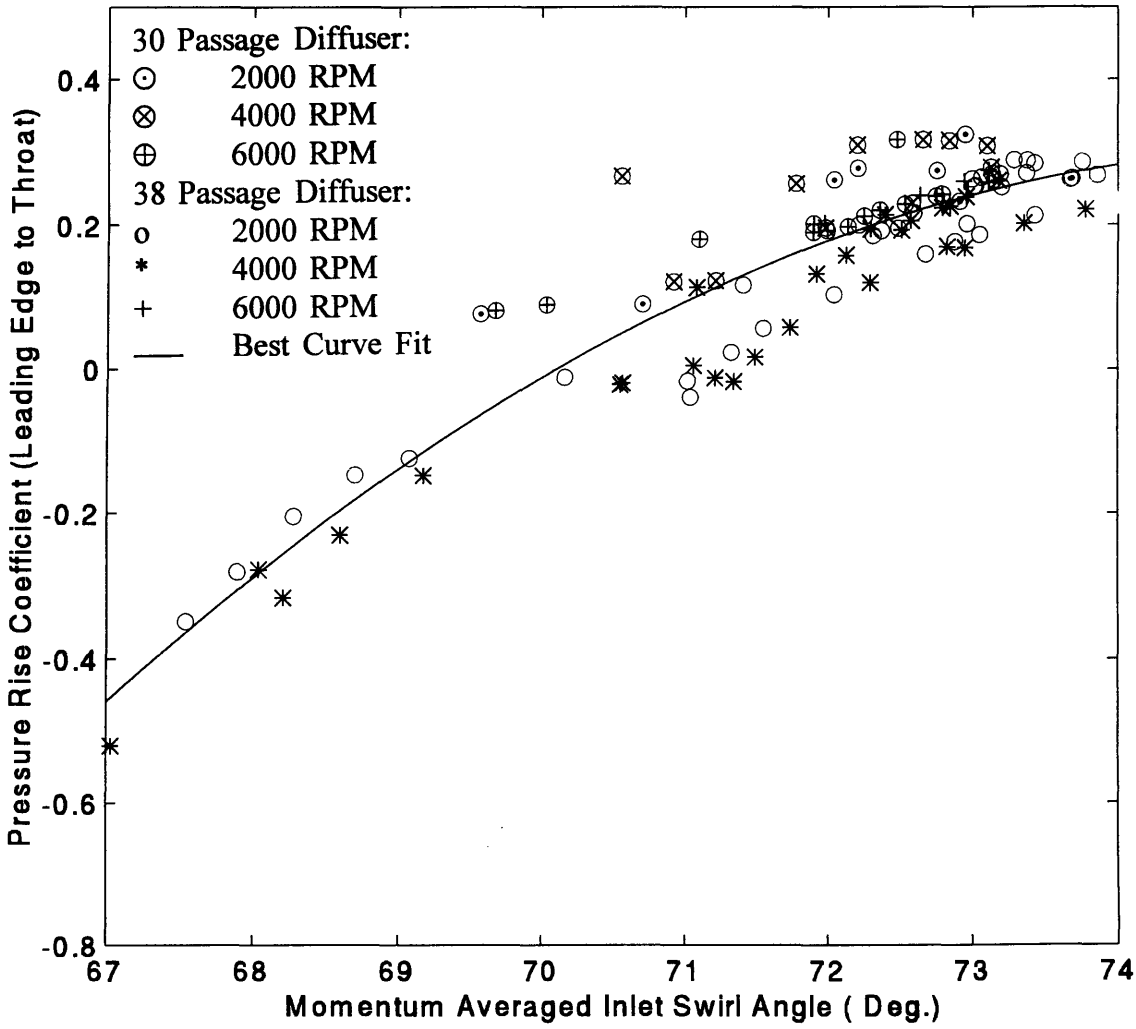

Figure 5.6: Static Pressure Rise Coefficient, Leading Edge to Throat, versus Inlet Swirl Angle.

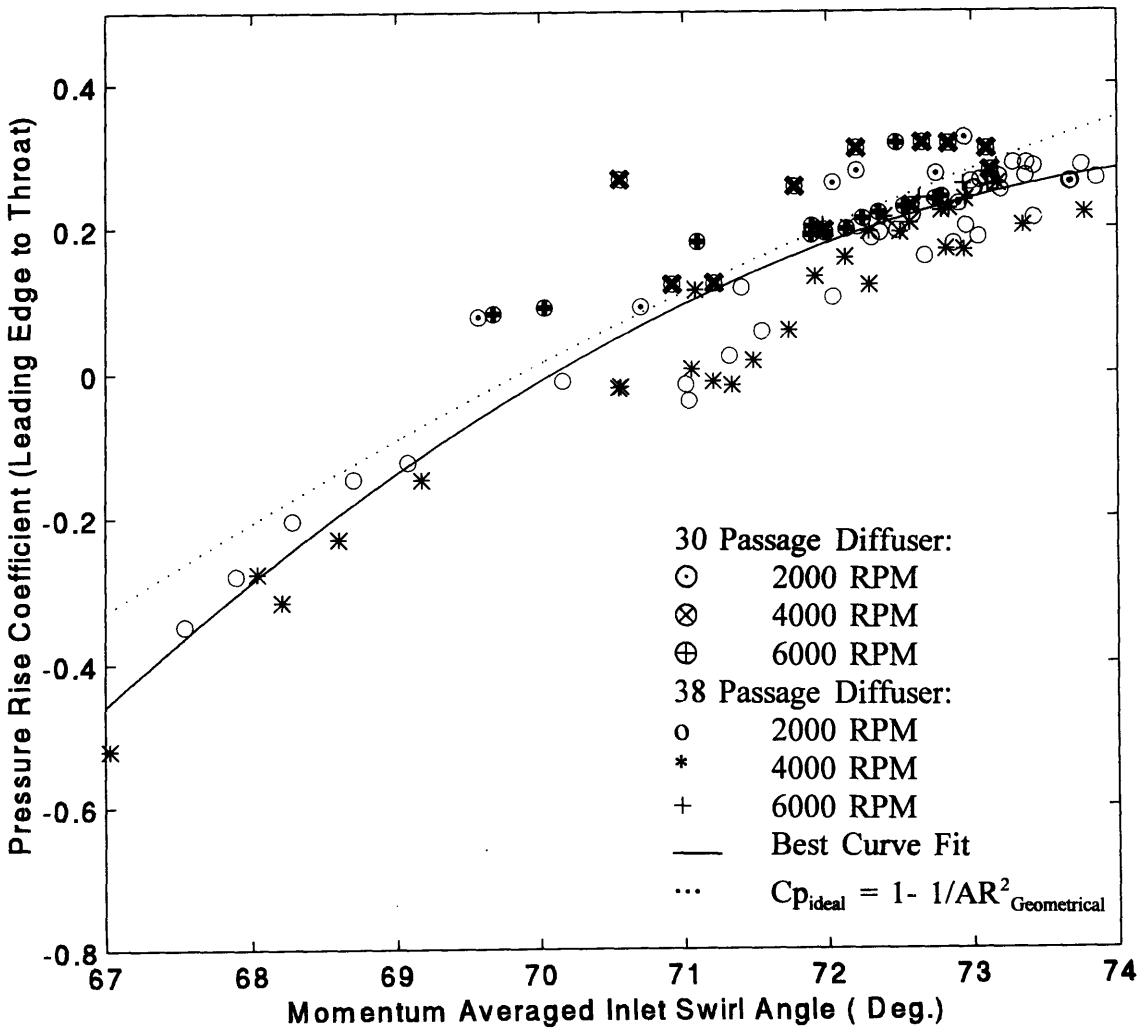

Figure 5.7: Static Pressure Rise Coefficient, Leading Edge to Throat, Versus Inlet Swirl Angle.

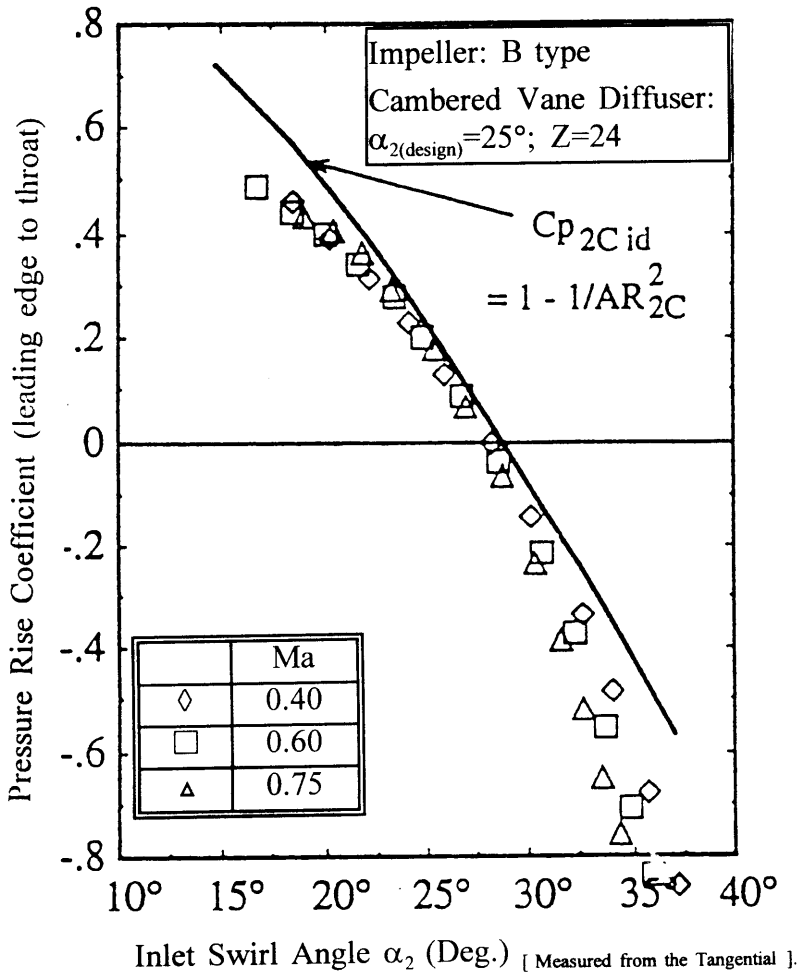

Figure 5.8: Static Pressure Rise, Leading Edge to Throat: Ideal versus Actual [8].

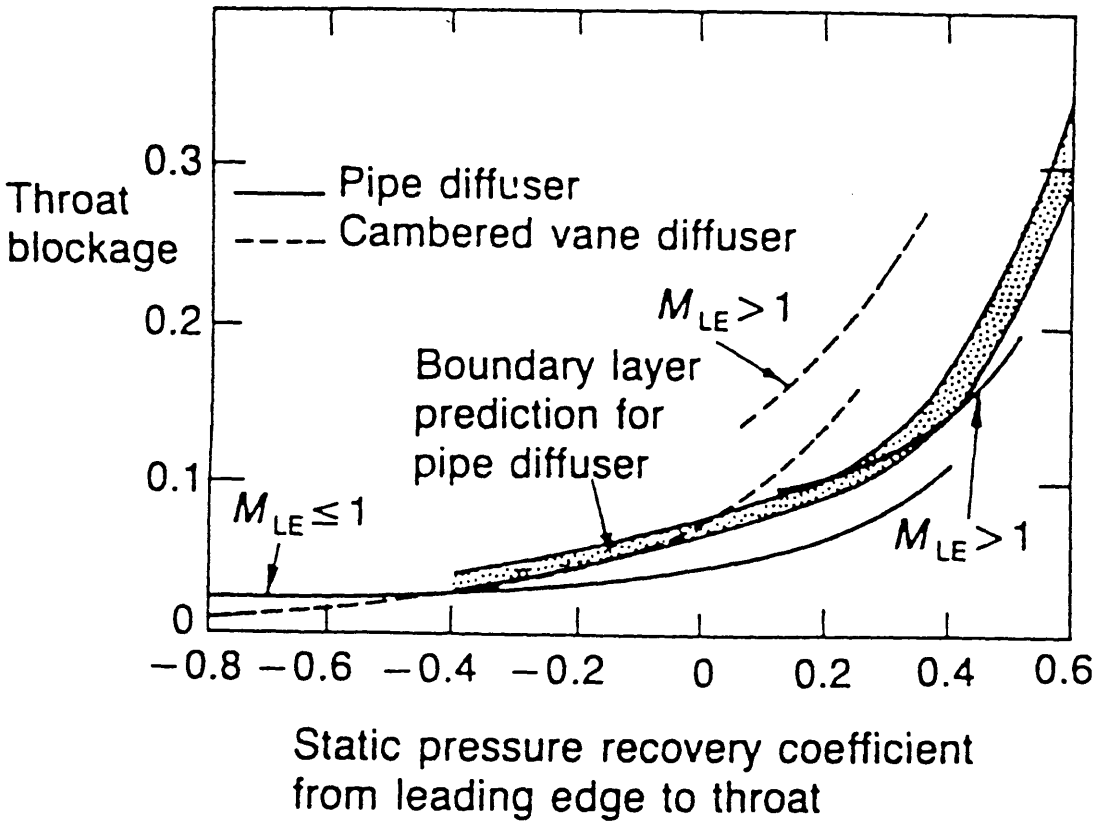

Figure 5.9: Kenny's Experimental Data on Pipe Diffusers for Throat Blockage versus Static Pressure Rise Coefficient, Leading Edge to Throat.

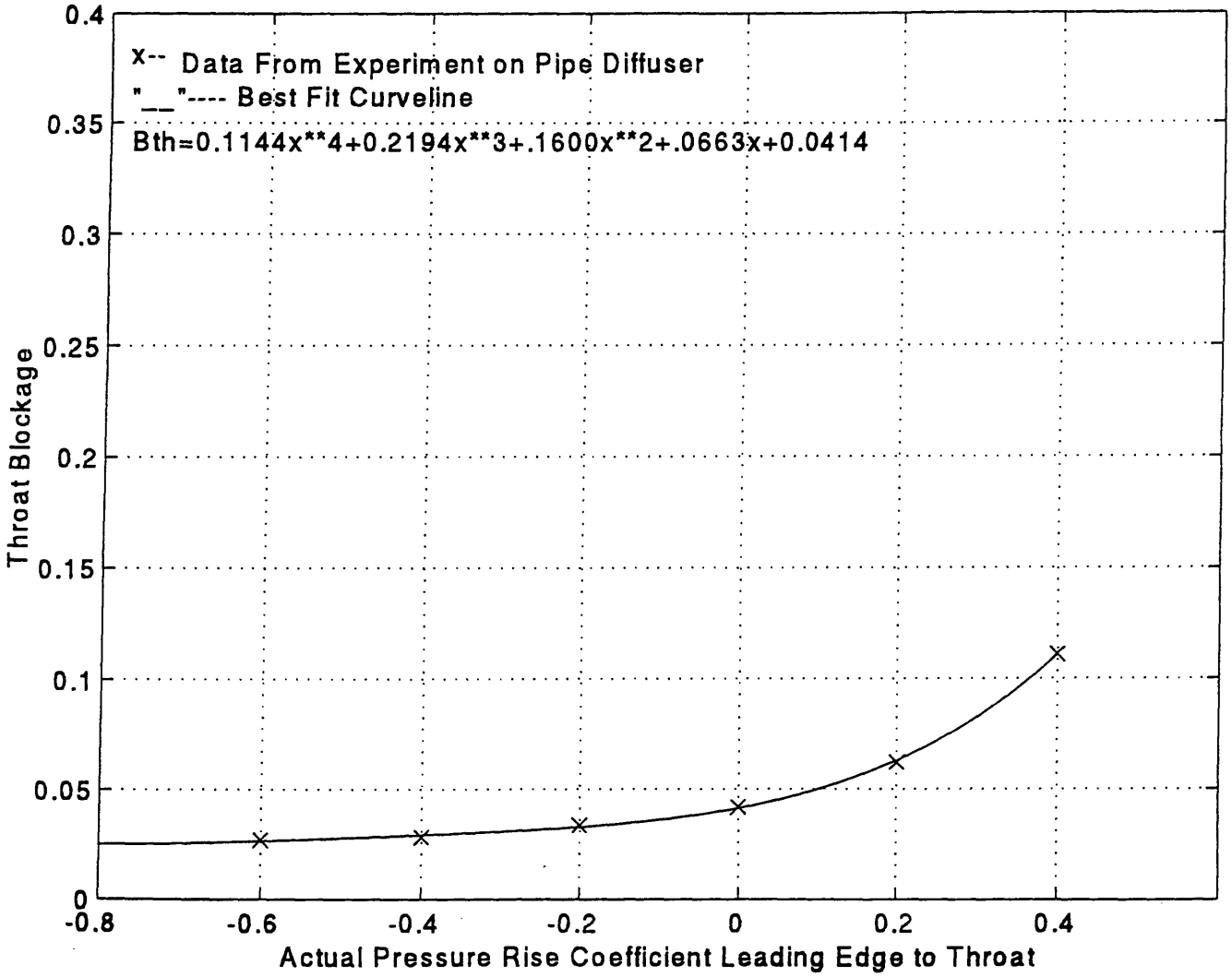

Figure 5.10: Empirical Relation Derived from Kenny's Experimental Data on Pipe Diffusers: Throat Blockage versus Static Pressure Rise Coefficient, Leading Edge to Throat.

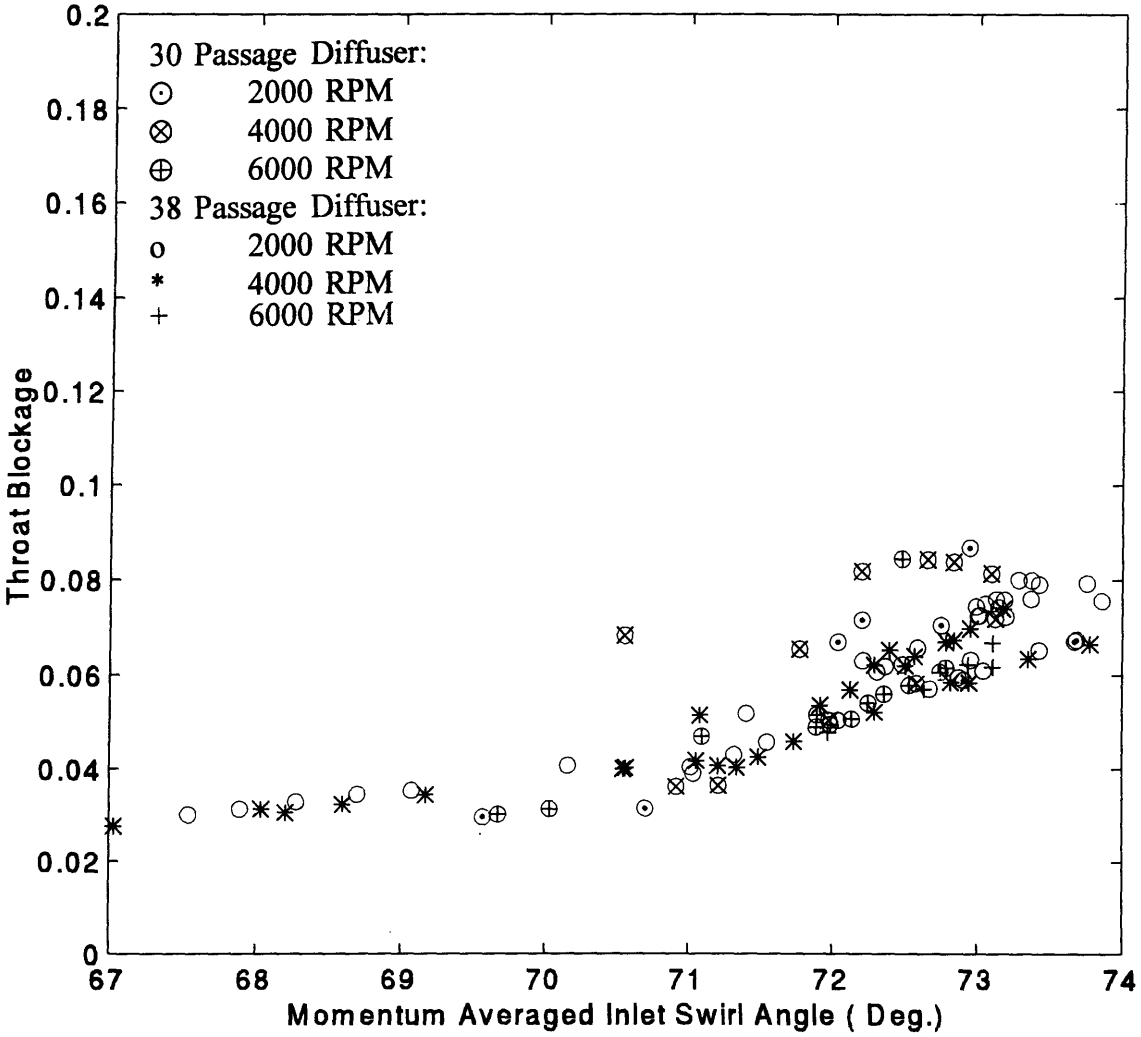

Figure 5.11: Throat Blockage versus Inlet Flow Angle (Deg.). for the two Discrete Passage Diffusers.

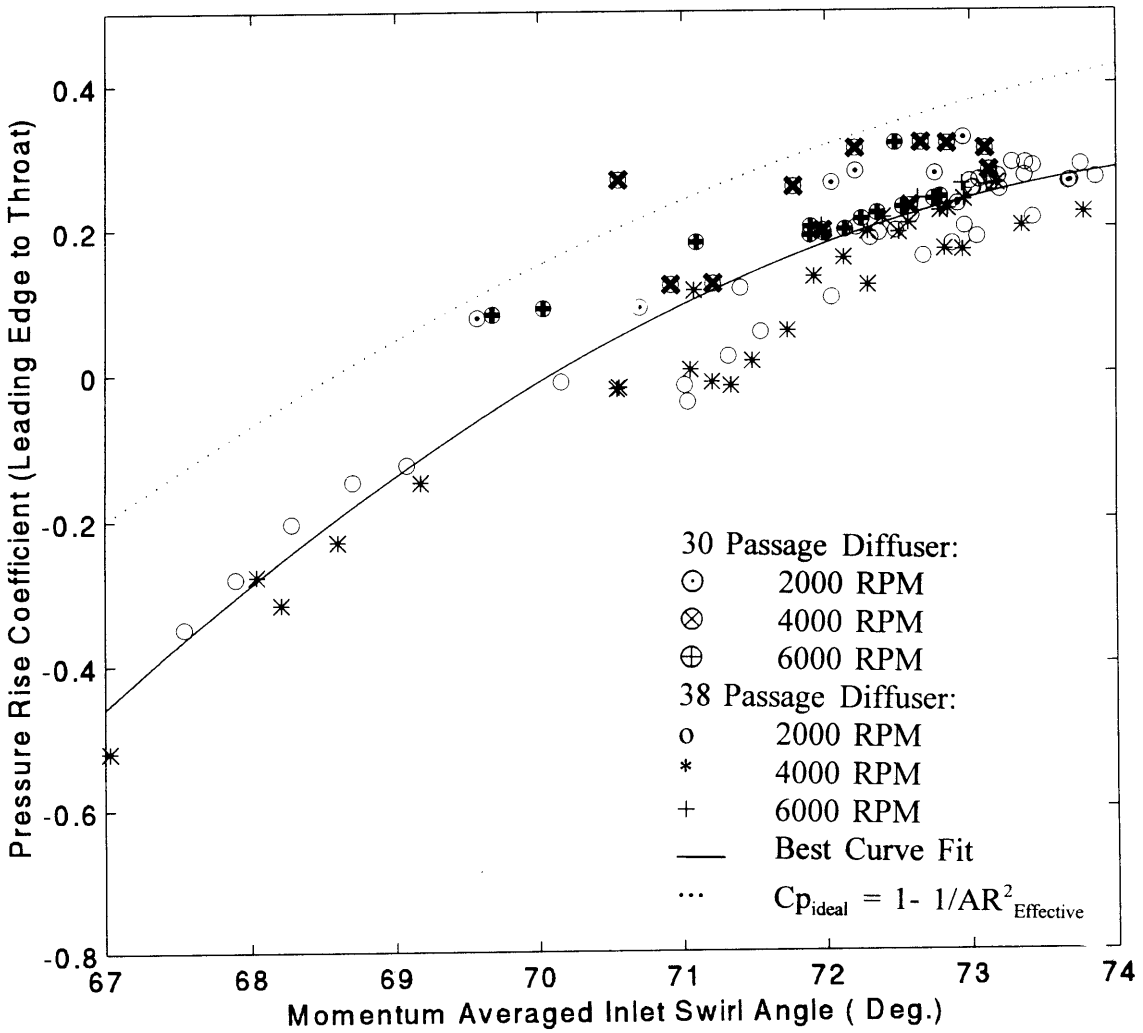

Figure 5.12: Static Pressure Rise Coefficient, Leading Edge to Throat, Ideal versus Actual. [Cp_{ideal} is computed with Effective Area Ratio].

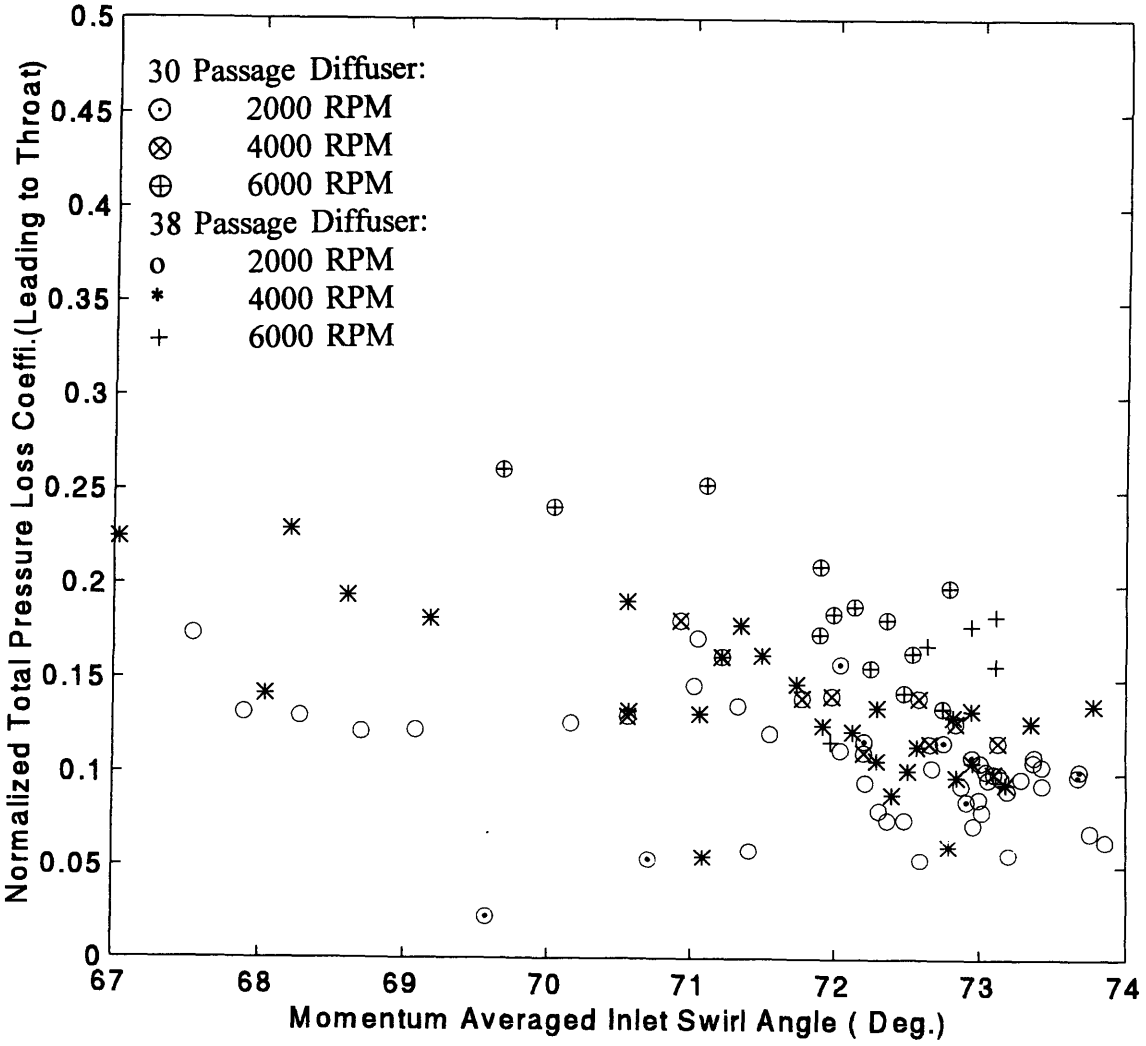

Figure 5.13: Total Pressure Loss, Leading Edge to Throat, Normalized by Inlet Dynamic Pressure, versus Inlet Swirl Angle..

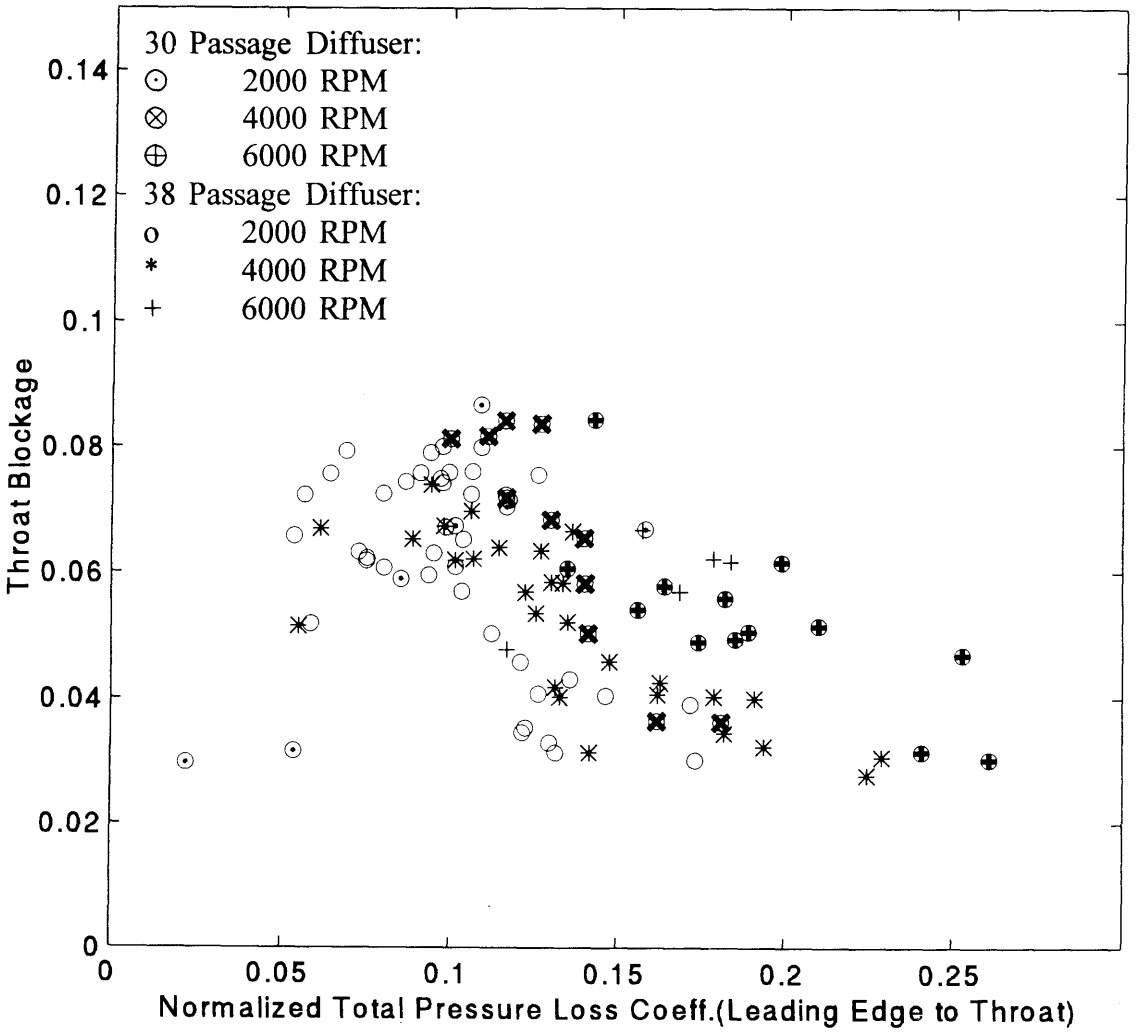

Figure 5.14: Throat Blockage versus Total Pressure Loss, Leading Edge to Throat, Normalized by inlet Dynamic Pressure.

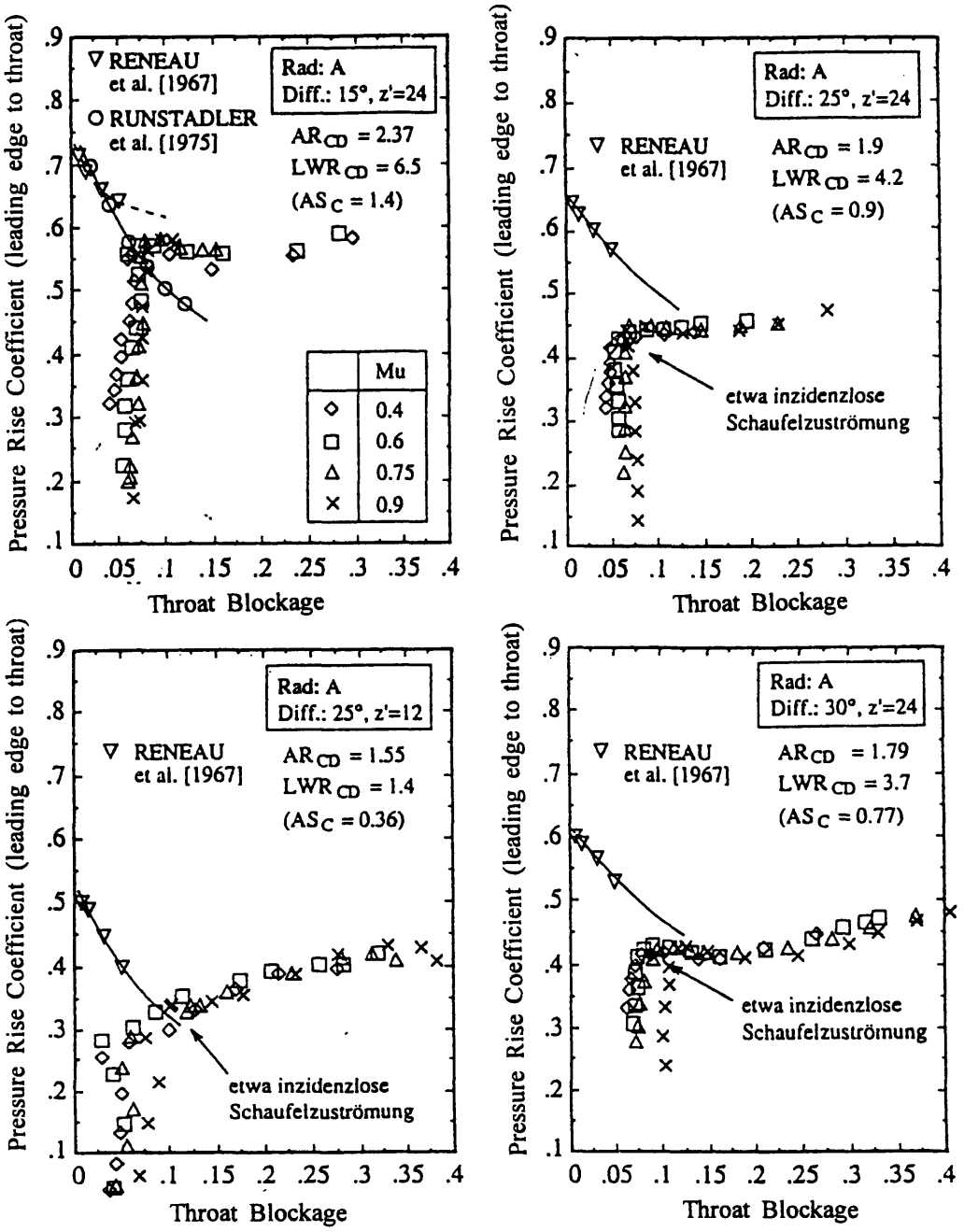

Figure 5.15: Pressure Rise Coefficient Cp′ versus Throat Blockage for various Vaned Diffusers [8].

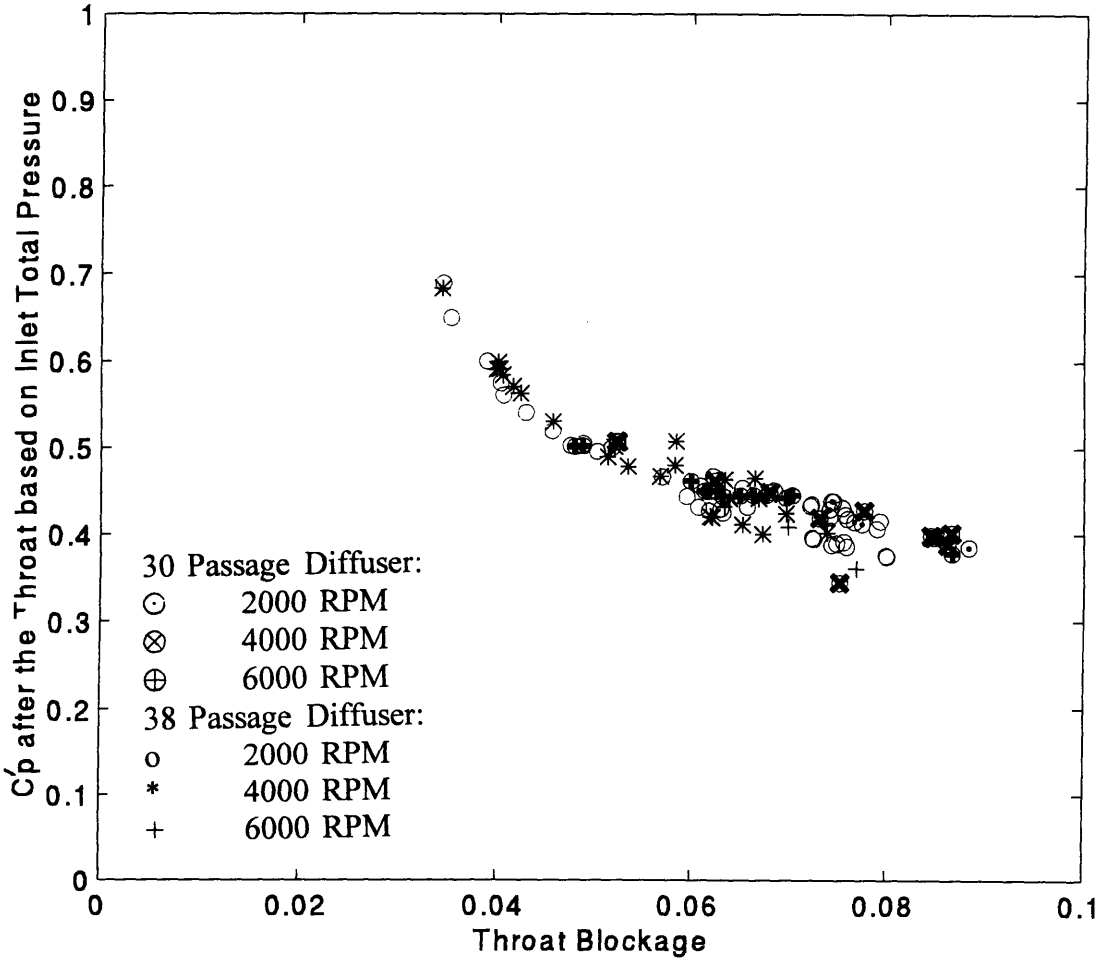

Figure 5.16: Pressure Rise Coefficient versus Throat Blockage for the two Discrete Passage Diffusers.

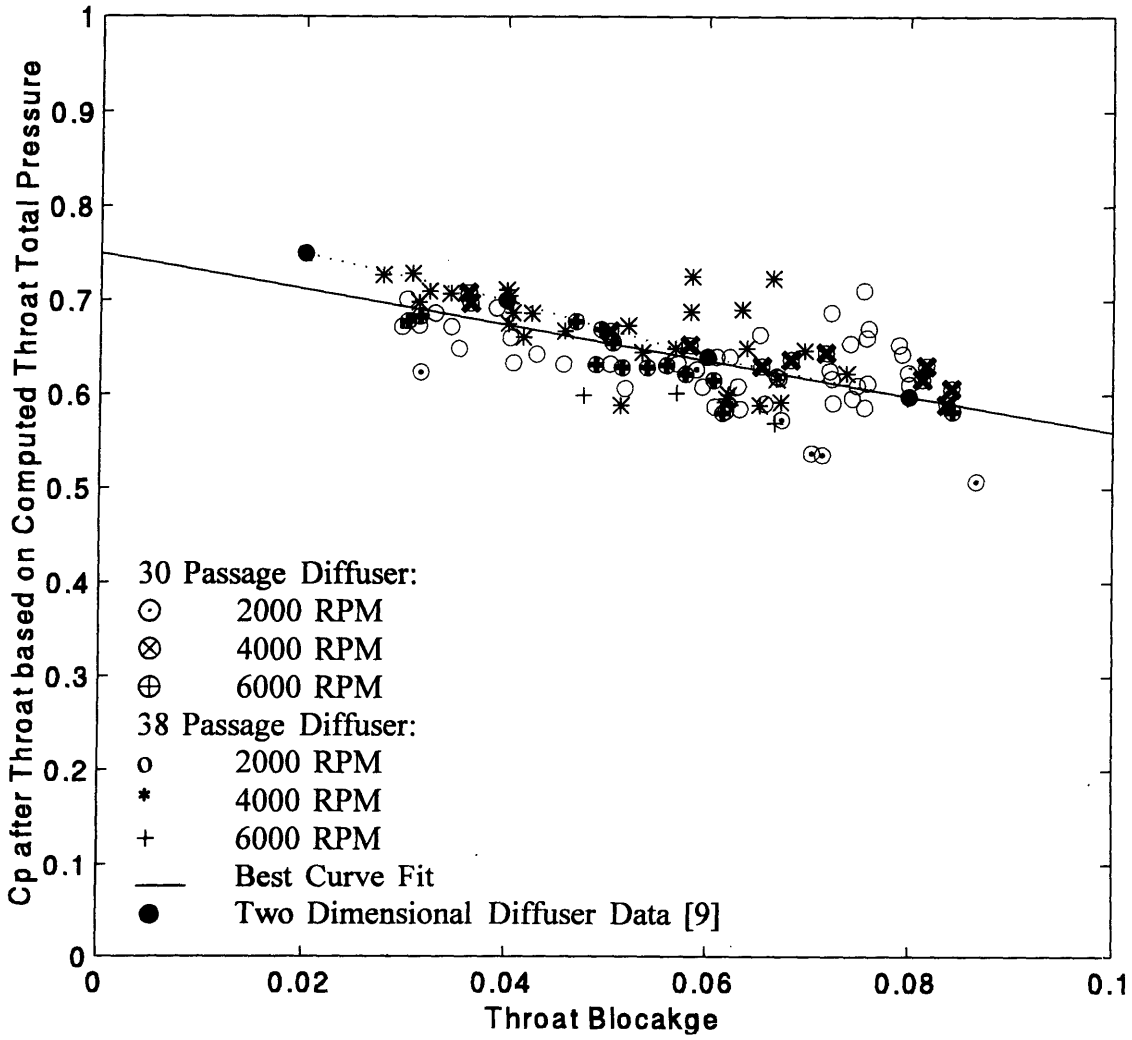

Figure 5.17: Pipe Diffuser Channel Performance versus two Dimensional Diffuser Performance

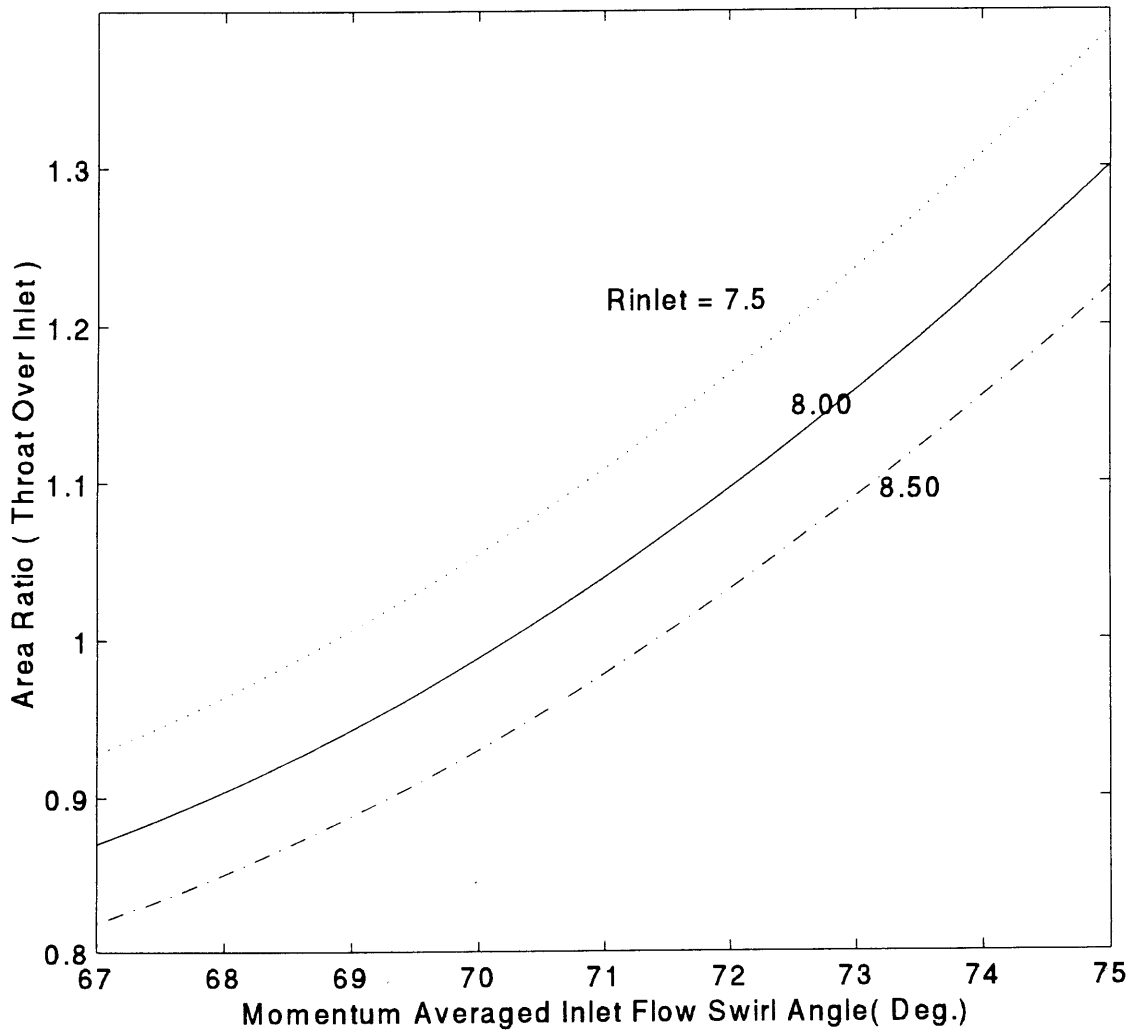

Figure 5.18: Geometric Area Ratio of Throat over Inlet with Different Radius versus Inlet Flow Swirl Angle (Deg.).

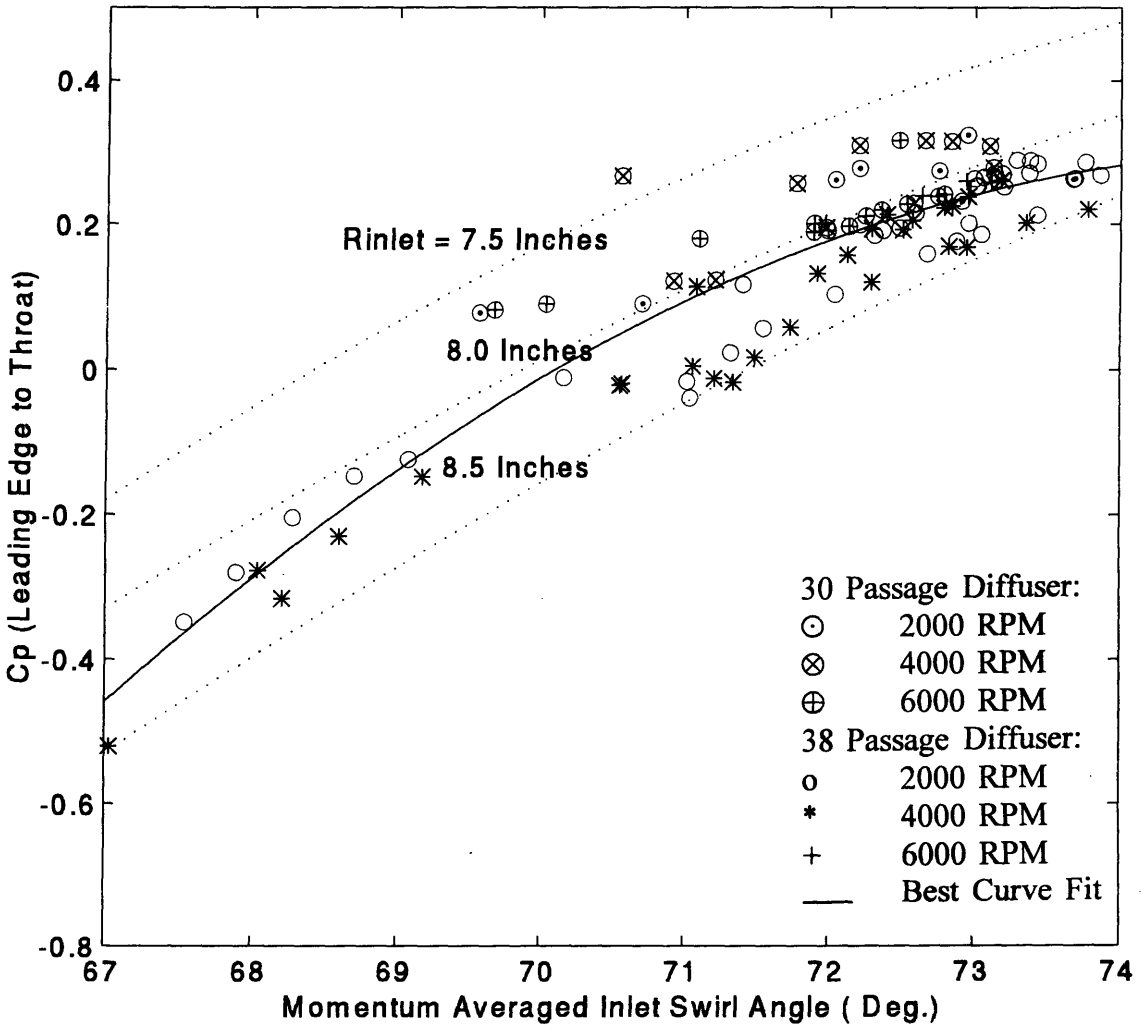

Figure 5.19: $Cp_{ideal} = 1 - 1/AR^2_{Geometric}$ at Different Inlet Radius versus Inlet Flow Swirl Angle (Deg.).

Chapter 6

Summary

The following results have been obtained relating to the flow in discrete passage diffuser for centrifugal compressor:

1. Throat blockage has been quantified.
2. The throat blockage is mainly determined by the momentum averaged inlet swirl angle.
3. There is little dependence of throat blockage on inlet blockage, also as shown by Filipenco[7] and Johnston[10], inlet blockage has little effect on the overall discrete passage diffuser pressure rise coefficient.
4. The measured static pressure rise coefficient, from the leading edge to the throat, has been found to be approximately equal to the value for lossless flow.
5. There is significant total pressure loss in the entry region. If this loss is taken into account when defining the pressure rise coefficient from diffuser throat to diffuser exit, the channel of a discrete passage diffuser behaves similar to a two dimensional straight channel diffuser.
6. For a given geometry, the pressure rise coefficient, from diffuser leading edge to diffuser throat is a function of momentum averaged inlet swirl angle only. Because the throat blockage is determined by the inlet swirl angle as well, the pressure rise coefficient of the channel part of a diffuser must also be determined by the

momentum averaged inlet swirl angle.

7. Once the geometry of a diffuser is given, the pressure rise coefficient for both parts, one from diffuser leading edge to the throat, the other from the throat to the exit, are entirely determined by the inlet swirl angle. Therefore the overall pressure rise coefficient is only a function of the momentum averaged inlet swirl angle.
8. One performance advantage of a discrete passage diffuser over an vaned diffuser may be that the inlet shape keeps the throat blockage low, presumeably by increasing mixing, which increases the static pressure recovery at the channel part of the discrete passage diffuser.
9. A method to predict the pressure rise of a discrete passage diffuser has been developed based on the above findings.

Reference:

1. Baghdadi, Samy, *A Study of Vaned Radial Diffusers Using Swirling Transonic Flow Produced By a Vortex Nozzle.* PhD Thesis, School of Mechanical Engineering, Purdue University, December 1973.

2. Baghdadi, Samy, *The Effect of the Rotor Blade Wakes on Centrifugal Diffuser Performance- A Comparative Experiment.* Journal of Fluids Engineering, pp 45-52, Vol. 99, March 1977.

3. Cumpsty, N.A., *Compressor Aerodynamics.* Longman Scientific & Technical Publisher, Essex, England, 1989.

4. Dean, Robert C., Jr., *The Fluid Dynamic Design of Advanced Centrifugal Compressors.* Creare Inc, Hanover, New Hampshire, TN-185, July 1974.

5. Dean, Robert C., Jr., *On the Unresolved Fluid Dynamics of the Centrifugal Compressor.* in *Advanced Centrifugal Compressors,* Copyright by ASME, pp. 1-55, 1971.

6. Dolan, Francis X. and Runstadler, Peter W., Jr., *Pressure Recovery Performance of Conical Diffusers at High Subsonic Mach Numbers.* NASA Technical Report CR-2299, August 1973.

7. Filipenco, Victor G., *Experimental Investigation of Flow Effects on the Performance of Radial Discrete-Passage Diffusers.* PhD Thesis, MIT, Department of Aeronautics and Astronautics, September 1991.

8. Hunziker, Rene, *The Influence of the Diffuser Geometry on the Instability Limit of Centrifugal Diffuser.* PhD Thesis, Swiss Federal Institude of Technology, Department of Mechanical Engineering, May 1993.

9. Japikse, D., *Turbomachinery Diffuser Design Technology.* The Design Technology Series DTS-1, Concepts ETI Inc., Norwich, Vermont, USA.

10. Johnston, John Mark, *Stall Onset Observation of Discrete Passage Diffuser.* S.M. Thesis, MIT, Department of Aeronautics and Astronautics, April 1993.

11. Kenny, D. P., *A Comparason of the Predicted and Measured Performance of High Pressure Ratio Centrifugal Compressor Diffusers.* ASME Paper 72-GT-54, 1972.

12. Kline, S. J. and Johnston, J. P., *Diffusers - Flow Phenomena and Design.* in *Advanced Topics* in *Turbomachinery Technology.* Concepts ETI Inc. Principal Lectures Series No. 2, Chapter 6, Copyright by Concepts ETI, Inc., Norwich, 1986.

13. Runstadler, Peter W., Jr., *Pressure Recovery Performance of Straight Channel, Single-Plane Divergence Diffusers at High Mach Numbers.* USAAVLABS, Technical Report 69-56, 1969.

14. Runstadler, Peter W., Jr., and Dean, Robert C., Jr., *Straight Channel Diffuser Performance at High Mach Numbers.* Transactions of the ASME, *Journal of Basic Engineering.* September 1969, pp. 397-422.

15. Wilson, D. G., *The Design of High Efficiency Turbomachinery and Gas Turbines.* The MIT Press, Cambridge, Massachusetts, 1984, pp. 147-187 and 241-243.

Appendix A

Total Pressure Loss from the Diffuser Leading Edge to the Diffuser Throat

To calculate the total pressure loss from leading edge to the diffuser throat, we need the total pressure of both the diffuser inlet and the diffuser throat. At the diffuser inlet, we know the static pressure and the total pressure, the mass flow rate. The total temperature, measured downstream of the diffuser, can be assumed to be constant across the diffuser, ie, from the leading edge to the exit of diffuser. We thus have the following known quantities:

at the diffuser inlet: $P_{t\psi 1}$, P_1, m_1, T_{01}, A_1

at the diffuser throat: P_{th}, m_{th}, T_{0th}, A_{th}

Based on these known quantities, using Equation A-1 below, we can find $Cp_{1\text{-}th}$, the static pressure rise coefficient from the diffuser leading edge to the diffuser throat.

$$Cp_{\psi}=\frac{P_2-P_1}{P_{t\psi 1}-P_1} \qquad \text{(A-1)}$$

Second, using Equation A-2, which is an empirical relation from Kenny's experimental data on pipe diffuser, we can calculate the throat blockage B_{th}.

$$B_{th}=.1144Cp_{1\text{-}th}^4+.2194Cp_{1\text{-}th}^3+.1600Cp_{1\text{-}th}^2+.0663Cp_{1\text{-}th}+.0414 \qquad \text{(A-2)}$$

Then, according to Equation A-3, the definition of blockage, we can

calculate the ideal mass flow rate at the throat, the flow rate when the blockage is zero.

$$B_{th}=1-\frac{m_{th}}{m_{th\,(ideal)}} \qquad \text{(A-3)}$$

Using the ideal mass flow rate at the diffuser throat, and the following two equations, A-4 and A-5, we can calculate the total pressure at the diffuser throat.

$$\frac{P_{tth}}{P_{th}}=\left(1+\frac{k-1}{2}M_{th}^2\right)^{\frac{k}{(k-1)}} \qquad \text{(A-4)}$$

$$m_{th\,(ideal)}=\left(\frac{P_{tth}}{RT_t}\right)\sqrt{kRT_t}M_{th}A_{th}\frac{1}{\left(1+\frac{k-1}{2}M_{th}^2\right)^{\frac{k+1}{2(k-1)}}} \qquad \text{(A-5)}$$

This requires iteration to solve for both total pressure P_{tth} and Mach number M_{th} at the diffuser throat.

The total pressure loss $\Delta P_{t(1\text{-}th)}$ can be found using the following equation:

$$\Delta P_{t(1-th)}=P_{t\psi 1}-P_{tth} \qquad \text{(A-6)}$$

Appendix B

Flow Chart to Predict the Pressure Rise Coefficient of a Discrete Passage of Given Geometries

The procedure to predict the pressure rise performance of a diffuser of given geometries has been discussed in section 5.3. Here is the flow chart of the procedure.

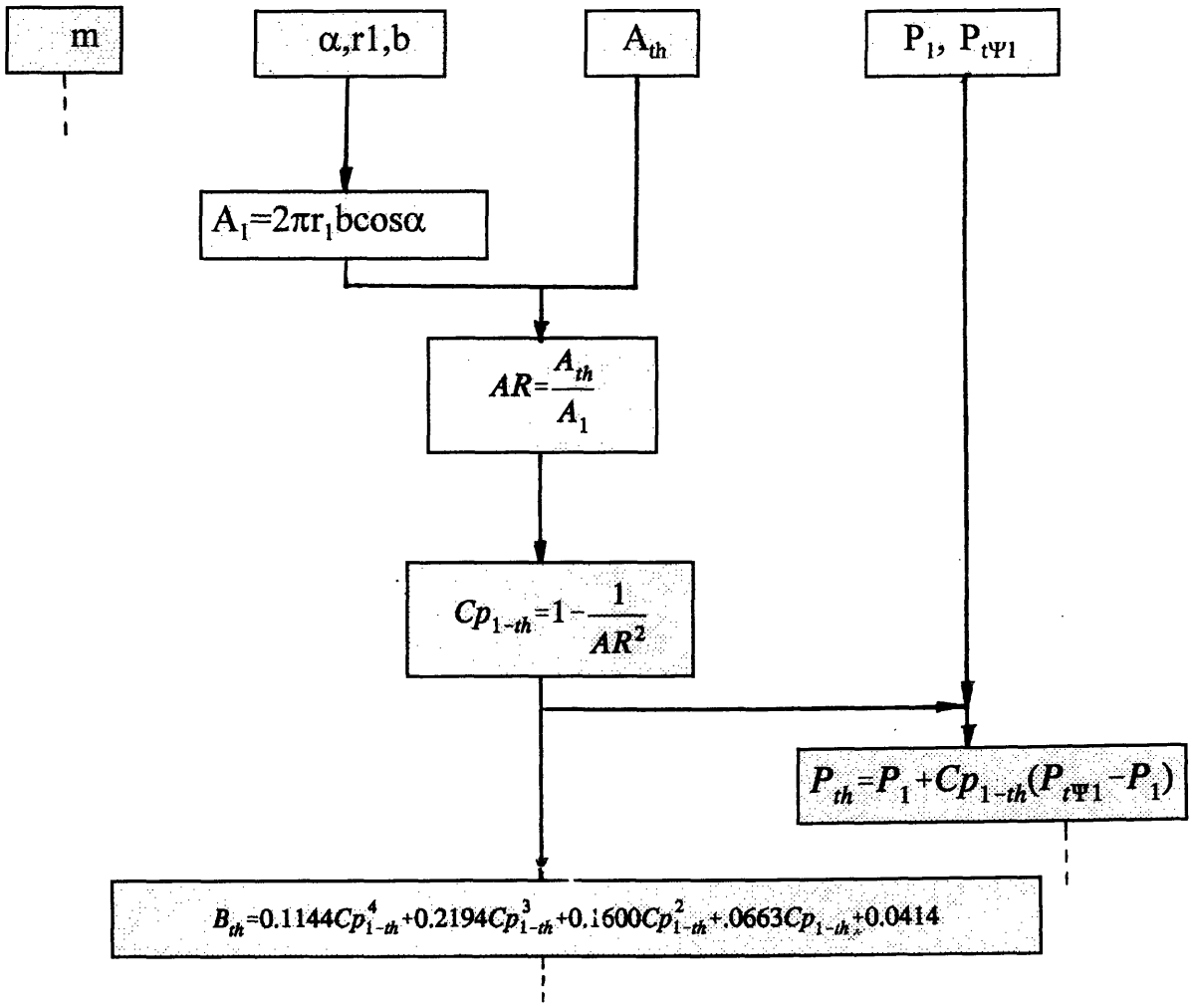

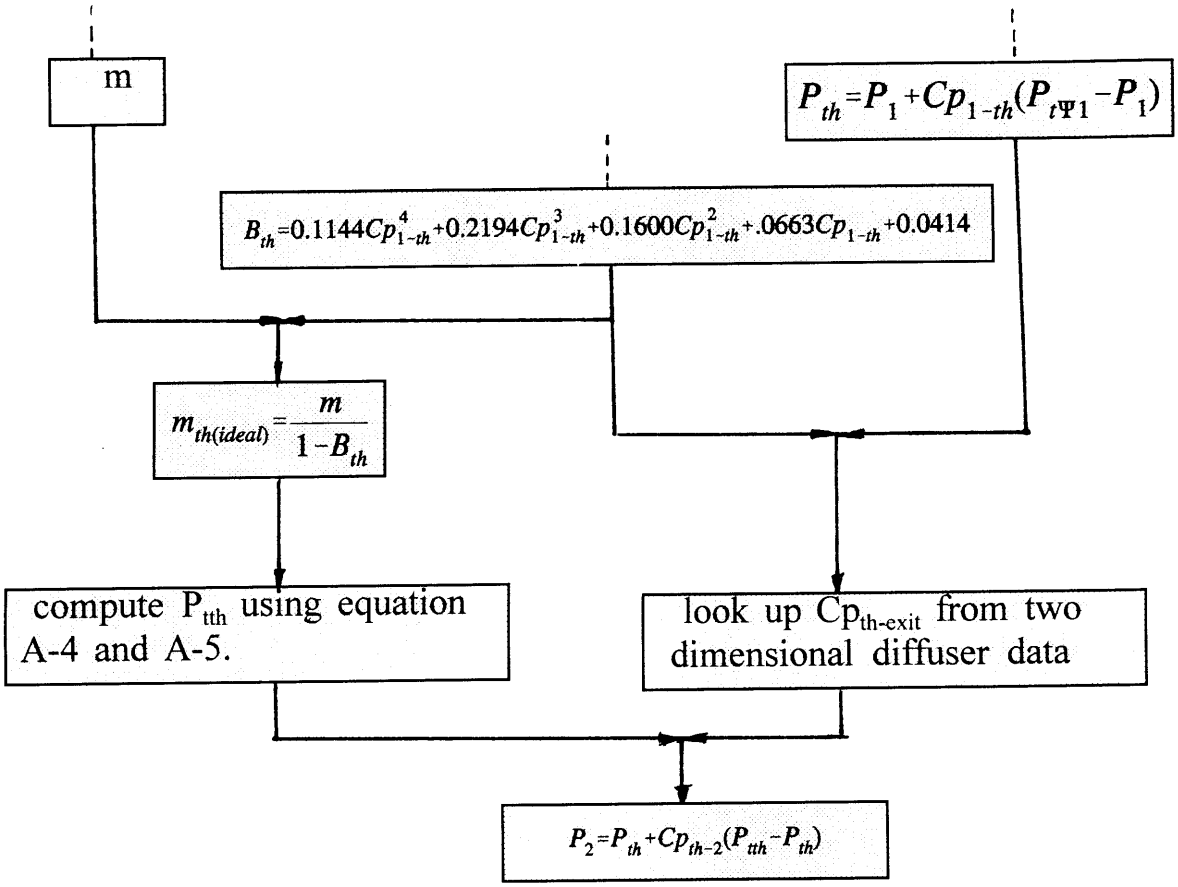
m
$P_{th}=P_1+Cp_{1-th}(P_{t\Psi 1}-P_1)$
$B_{th}=0.1144Cp_{1-th}^4+0.2194Cp_{1-th}^3+0.1600Cp_{1-th}^2+.0663Cp_{1-th}+0.0414$
$m_{th(ideal)}=\frac{m}{1-B_{th}}$
compute P_{tth} using equation A-4 and A-5.
look up $Cp_{th\text{-}exit}$ from two dimensional diffuser data
$P_2=P_{th}+Cp_{th-2}(P_{tth}-P_{th})$